Copy 6
RM E55A27

RESEARCH MEMORANDUM

DESIGN AND PERFORMANCE OF A 1400-FOOT-PER-SECOND-TIP-SPEED SUPERSONIC COMPRESSOR ROTOR

By John F. Klapproth, John J. Jacklitch, Jr., and Edward R. Tysl

Lewis Flight Propulsion Laboratory
Cleveland, Ohio

NATIONAL ADVISORY COMMITTEE
FOR AERONAUTICS

WASHINGTON

April 11, 1955

[redacted]

NATIONAL ADVISORY COMMITTEE FOR AERONAUTICS

RESEARCH MEMORANDUM

DESIGN AND PERFORMANCE OF A 1400-FOOT-PER-SECOND-TIP-SPEED SUPERSONIC COMPRESSOR ROTOR

By John F. Klapproth, John J. Jacklitch, Jr.,
and Edward R. Tysl

SUMMARY

A supersonic compressor was designed for a tip speed of 1400 feet per second, a pressure ratio of 2.0, and a corrected weight flow of 30.5 pounds per second. The rotor was designed for equal distribution of static-pressure diffusion across the rotor and the stator based on recovery of the relative inlet dynamic head. Rotor-blade profiles and hub contour were obtained from a channel-flow design approach. Maximum blade thickness was $4\frac{1}{2}$ percent chord.

Over-all performance results of the rotor alone at design speed gave a pressure ratio of 2.17, an adiabatic efficiency of 89 percent, and a weight flow of 28 pounds per second. Maximum efficiency of 94 percent was observed at 82 percent design speed with a pressure ratio of 1.65. Performance characteristics were similar to those of conventional subsonic and transonic rotors with a range in weight flow at good efficiency for all speeds.

Inlet relative Mach numbers were supersonic across the entire blade span for speeds of 90 percent design and above. There were no appreciable effects of Mach number on blade-element losses below 90 percent of design speed. At 90 percent design speed and above, there was an increase in the relative total-pressure losses at the tip. However, based on rotor diffusion factor, these losses for Mach numbers up to 1.35 are comparable with the losses in subsonic and transonic compressors at equivalent values of blade loading.

INTRODUCTION

The investigations of supersonic axial-flow compressors (i.e., compressors having supersonic velocities relative to any blade row, refs. 1

[redacted]

and 2) have been confined largely to two different types. The shock-in-rotor compressor with subsonic stators was considered as being capable of pressure ratios up to about 3:1. The impulse type with supersonic velocities throughout the high-turning rotor passages to give supersonic velocities entering the stator is theoretically capable of very high stage pressure ratios of 8 and above (refs. 3 and 4).

Experimental performance of the shock-in-rotor type has generally shown poor rotor performance with observed pressure ratios well below design and a severe redistribution of the flow toward the root (refs. 5 to 9). Performance has generally been so poor as to make stage tests of little interest.

The experimental results of the impulse-type rotors when tested alone have shown that high energy input can be accomplished with a reasonable efficiency (refs. 10 to 12). The energy imparted, however, is almost entirely in the form of kinetic energy with stator-inlet Mach numbers well above 1.0. Attempts to convert this into pressure by deceleration through Mach 1.0 in the stators have resulted in severe reductions in efficiency and pressure ratio (refs. 13 to 15).

The distribution in static-pressure rise across the rotor and the stator for both types is considerably different than that usually obtained in subsonic compressors (e.g., for the symmetrical velocity diagram where the static-pressure rise is distributed equally across rotor and stator). The shock-in-rotor compressors were frequently designed for a larger static-pressure ratio across the rotor than total-pressure ratio across the stage. For the impulse-type rotor, the design static-pressure ratio across the stators was very nearly equal to the stage total-pressure ratio.

The poor performance of the supersonic-compressor types previously discussed can be attributed largely to flow separation which, in turn, results from attempts to obtain too high a static-pressure rise across the blade row. Improvement in performance of supersonic compressors can be anticipated if the static-pressure rise across the blade row is limited to values less than those associated with shock boundary-layer interactions that lead to flow separation (refs. 16 and 17). In addition, the highest pressure ratios consistent with good efficiency will be obtained when the maximum static-pressure rise without separation is obtained across both the rotor- and stator-blade rows. This report presents (1) the general considerations leading to the selection of a rotor design point based on a distributed static-pressure rise across both the rotor and the stator, (2) the design of the rotor, and (3) the over-all and blade-element performance of the rotor alone.

SYMBOLS

The following symbols are used in this report:

a,b	constants used in describing blade mean line
D	diffusion factor
ΔH	work input
h	ratio of stream-filament thickness to stream-filament thickness at inlet to compressor
i	incidence angle, deg
M	absolute Mach number, ratio of absolute gas velocity to local velocity of sound
M'	relative Mach number, ratio of gas velocity relative to rotor to local velocity of sound
M_T	tip speed, made dimensionless by inlet stagnation velocity of sound
n	number of blades
P	total pressure, made dimensionless by upstream stagnation pressure
P'	relative total pressure, made dimensionless by upstream stagnation pressure
p	static pressure, made dimensionless by upstream stagnation pressure
Q	velocity ratio, made dimensionless by upstream stagnation velocity of sound
R	radius ratio, radius r made dimensionless by tip radius
r	radius, in. or ft
∂s	differential in distance along streamline, made dimensionless by tip radius
t	blade thickness, made dimensionless by tip radius
U	rotational speed, ft/sec
V	absolute velocity, ft/sec
V'	velocity relative to blade row, ft/sec

[redacted]

W	weight flow, lb/sec
x	axial distance, in.
z	axial dimension, made dimensionless by tip radius
β	absolute air-flow angle measured from axis of rotation
β'	relative air-flow angle measured from axis of rotation
γ	ratio of specific heats
δ	ratio of inlet total pressure to NACA standard sea-level pressure
δ°	deviation angle, deg
η	adiabatic efficiency
θ	ratio of inlet total temperature to NACA standard sea-level temperature
θ°	air turning angle, change in relative flow angle from inlet to outlet of blade row
$d\theta$	differential in tangential direction (positive in direction of rotation)
ρ	density made dimensionless by upstream stagnation density
σ	blade solidity
φ	angle between streamline and axis of rotation measured in Rz plane
ψ	dimensionless static-pressure recovery, $\frac{p_2 - p_1}{p_1' - p_1}$ or $\frac{p_3 - p_2}{p_2 - p_2}$
$\bar{\omega}$	relative total-pressure loss coefficient (ref. 18)

Subscripts:

h	hub
m	mean condition on mean streamline
p	pressure surface of blade

[redacted]

R	rotor
r	radial component
S	stator
s	suction surface
t	tip
z	axial component
θ	tangential component
0	station in inlet plenum tank
1	station at rotor inlet
2	station 1 in. downstream of rotor
3	station 9.7 in. downstream of rotor

COMPRESSOR DESIGN

General considerations. - The range of pressure ratios theoretically available at a rotor speed of 1400 feet per second with no guide-vane turning and an axial inlet Mach number of 0.7 is shown in figure 1(a). The isentropic total-pressure ratio is plotted against the rotor turning angle for various values of rotor-outlet relative Mach number. Values are shown for the dimensionless static-pressure recovery ψ, defined as the ratio of the static-pressure rise to the difference between the inlet relative total pressure and the inlet static pressure. Contours of constant static-pressure recovery in the stators resulting when the stators diffuse to the rotor-inlet absolute Mach number are also shown.

Shock-in-rotor supersonic-compressor designs have generally been characterized by a diffusion to subsonic relative outlet Mach numbers of about 0.7 with only moderate rotor turning. This design is seen from figure 1(a) to result in large amounts of diffusion ($\psi_R \sim 0.6$). If the stators are designed for an outlet Mach number equal to the absolute rotor-inlet Mach number, then, from figure 1(a), ψ_S is very small and can even be negative. The impulse rotors have been characterized by a large amount of turning in the rotor with very little rotor diffusion. A large amount of diffusion is then required in the stators.

[redacted]

From the standpoint of a complete stage, a more reasonable design would be to distribute the static-pressure rise across both the rotor and the stator. In general, the Mach numbers relative to the rotor- and stator-blade rows can be considerably different. Under these circumstances a reasonable method of distribution would be on the basis of ψ, the recovery of the relative inlet dynamic pressure.

The theoretical total-pressure ratios available with rotor speeds from 800 to 1600 feet per second for the case of equal static-pressure recovery across rotor and stator are shown in figure 1(b) plotted against rotor turning angle. These curves are based on equal Mach numbers at the inlet and outlet of the stage. Contours of constant pressure recovery and stator-inlet angle are also shown. The pressure ratio that can be obtained efficiently at any given rotor speed will then depend upon the maximum static-pressure recovery that can be obtained without flow separation.

Low-speed cascade data indicate that an increase in losses occurs with pressure recoveries above about 0.4 to 0.6 (fig. 3(e), ref. 18) with considerable variations at different staggers and solidities. A more desirable loading parameter was found to be a diffusion factor defined as (ref. 18)

$$D = 1 - \frac{V_2'}{V_1'} + \frac{\Delta V_\theta'}{2\sigma V_1'}$$

Cascade data indicated that a sharp rise in losses occurred for diffusion factors above about 0.6. In addition, rotor loss data, when compared with D for the rotor tip, indicated that a significant rise in tip losses occurred at about 75 percent of the two-dimensional cascade limiting value. A corresponding reduction in allowable tip loading can be expected by using a pressure recovery as a loading parameter. A direct relation does not exist between ψ and D for the general case since a blade-loading term and solidity are involved in D and not in ψ. However, for the conditions of constant axial velocity, inlet flow angle of 60°, and solidity of 1.0 (which is representative of tip condition), a reduction in D from 0.6 to 0.45 has a corresponding reduction in ψ from 0.6 to 0.48. Thus, a design utilizing a pressure recovery of about 0.3 to 0.4 can be expected to give reasonable performance. In view of the better correlation of losses with diffusion factor, the design should be reevaluated using the diffusion factor for both the rotor and the stator, once the solidity and axial-velocity ratios have been selected.

For the rotor used in this investigation, a pressure recovery of 0.33 was selected, equal in both rotor and stator, with the stator-outlet Mach number equal to the rotor-inlet Mach number. For the design tip speed of 1400 feet per second, this resulted in a rotor work input corresponding to an isentropic total-pressure ratio of 2.3 (fig. 1(b)).

Rotor-blade shape. - The selection of the rotor tip speed of 1400 feet per second, the axial inlet Mach number of 0.7, and the static-pressure recovery of 0.33 in both rotor and stator tip resulted in the following rotor relative inlet and outlet conditions at the tip:

	Inlet	Outlet
Mach number	1.487	1.04
Flow angle, deg	61.93	44.02

This combination of Mach number and angle change requires an appreciable contraction of the flow annulus in order to satisfy continuity. If a 10-percent allowance at the outlet is made for the blade wake and boundary layer, then the outlet passage height along the tip streamline must be reduced to 61 percent of the height at the inlet.

The requirement of an appreciable contraction of the annular passage height, in addition to the mixed subsonic and supersonic flow field that will exist, makes an accurate computation of a blade shape from a prescribed loading distribution or a desired flow pattern impractical if not impossible at present. Consequently, an approximate design system based on the channel-flow approach (ref. 19) was applied. The procedure followed very closely that described in reference 11.

The method of solution utilizes two equations: (1) the continuity equation in the form

$$\frac{R_1 \rho_1 Q_1 \cos \beta_1}{\sqrt{1 + \cos^2 \beta_1' \tan^2 \varphi_1}} = \frac{R \rho_m Q_m h \cos \beta'}{\sqrt{1 + \cos^2 \beta' \tan^2 \varphi}} \left(1 - \frac{nt}{2\pi R}\right) \tag{1}$$

and (2) an equation developed from the condition of zero absolute circulation (ref. 20)

$$\frac{n(Q_s - Q_p)}{2\pi} = \frac{\cos \beta'}{\sqrt{1 + \cos^2 \beta' \tan^2 \varphi'}} \frac{d}{dz} \left(\frac{Q_m \sin \beta'}{\sqrt{1 + \cos^2 \beta' \tan^2 \varphi}} + M_T R \right) R \left(1 - \frac{nt}{2\pi R}\right) \tag{2}$$

The mean velocity is assumed equal to the arithmetic average of the blade surface velocities, and the flow angles at any axial position are assumed equal to the mean flow angle.

These two equations involve five variables: (1) the mean-velocity distribution, (2) the mean flow angle, (3) the blade thickness distribution, (4) the annular contraction of the stream tube height, and (5) the blade surface-velocity distribution. For the rotor reported herein, the

mean-velocity distribution was prescribed. The mean flow angles and the blade thickness distribution were prescribed initially and modified as necessary to obtain an acceptable annular contraction of an incremental stream tube and the blade surface-velocity distribution. In order to match the prescribed inlet and outlet relative Mach numbers, the mean-velocity distribution requires a reduction in Mach number from 1.487 at the entrance to very close to 1.0 at the exit. The attainment of this deceleration in actual flow without shocks in a uniformly convergent passage is impossible in a two-dimensional open-throat-type diffuser (ref. 21) because of stability requirements. However, the use of a spiked-diffuser principle, whereby the flow is decelerated ahead of the closed or covered portion of the rotor-blade passage, should be applicable (ref. 8). Consequently, a mean-velocity distribution simulating that occurring in a cascade utilizing the spiked-diffuser principle was prescribed as one of the conditions. The resulting distribution required a rapid deceleration starting at the blade leading edge, as shown in figure 2(a), where the mean velocity at the rotor tip, shown as a ratio of the relative velocity to the upstream absolute stagnation sonic velocity, is plotted against the axial distance through the rotor.

3381

A linear variation of tangent β' between the inlet flow angle and the desired outlet flow angle was specified as

$$\frac{\tan \beta'}{R} = \frac{d\theta}{dz} = a + bz \tag{3}$$

The constants a and b were determined to satisfy the prescribed inlet and outlet angles. The resultant flow path at any radial section is then parabolic.

The blade thickness and streamline contraction through the channel were obtained from the continuity equation, and they had the final distributions shown in figures 2(b) and (c). The blade surface velocities may be estimated by using equation (2). The blade-loading distribution for 19 rotor blades is shown in figure 3.

The flow mean line for all streamlines other than at the tip were obtained by recomputing the constants a and b of equation (1) to match the inlet and outlet angles. The outlet angle was obtained from the requirement of equal work input along the radius. The thickness distribution shown in figure 2(b) was used for all sections.

In order to obtain the rotor-blade shape from the prescribed thickness distribution and the flow mean line, an incidence angle of $2\frac{1}{2}^\circ$ was assumed (based on the results of ref. 22). The blade mean line was faired forward from $z = 0.15$ (the approximate location of the entrance to the closed or covered part of the passage) to a value $2\frac{1}{2}^\circ$ less than the desired inlet flow angle at the leading edge. The boundary-layer allowance was

made entirely on the suction face of the blade, with the growth arbitrarily assumed to vary parabolicly along the blade surface. The blade shape, shown in figure 4, had a maximum thickness approximately $4\frac{1}{2}$ percent of the chord with the position of maximum thickness about 50 percent of the chord from the leading edge.

Hub contour. - The hub contour was obtained by computing successive stream filaments from the tip toward the hub. The conditions of radial equilibrium in the form

$$\frac{1}{\gamma\rho}\frac{\partial p}{\partial R} = \frac{(M_T R + Q_\theta)^2}{R} - Q\frac{\partial Q_r}{\partial s} \tag{4}$$

and continuity in the meridional plane based on the mean flow conditions were satisfied in the same manner as described in reference 11. The hub contour resulting from these calculations is shown in figure 4(b). The blade coordinates and hub contour defined in figure 4(a) are shown in table I.

APPARATUS AND INSTRUMENTATION

Compressor rotor. - The compressor rotor (fig. 5) was machined from a solid 14S-T aluminum forging. The rotor had a constant tip diameter of 16 inches, 19 blades, and an axial depth of 2.48 inches. The entrance hub radius ratio was 0.7; the tip solidity was 1.3. The compressor did not have inlet guide vanes or exit stators.

Compressor test rig. - The compressor test rig (fig. 6) consisted of an inlet tank (7.5 ft in diam. and 15 ft long), the compressor test section, the outlet-air collector, and the inlet and exhaust ducting.

The rig could be supplied with either refrigerated air or room air which was exhausted to either the altitude or atmospheric exhaust system.

The compressor was driven by a 6000-horsepower variable-frequency electric motor through a speed-increaser gear box.

Instrumentation. - Standard instrumentation was installed in the inlet tank to measure the inlet stagnation pressures and temperatures according to the method described in reference 23. Survey data were taken at eight radial positions at each of two stations downstream of the rotor. The stations were located approximately 1 inch and 9.7 inches downstream of the intersection of the blade trailing edge and the rotor hub. The data taken and the instruments used to obtain the data at each station are: (1) static pressure by a self-balancing L static probe, (2) total

pressure and flow angle with a combination probe at station 2 and a miniature claw probe at station 3, (3) total temperature with a self-balancing spike-type thermocouple probe, and (4) static pressures by four taps approximately 90° apart in both the inner and outer walls.

Fifty-three pressure taps were located in the outer wall to read the static pressures from 4 inches upstream to 13 inches downstream of the rotor leading edge. These taps were 1/4 inch apart in the vicinity of the rotor and instrument measuring stations and 1/2 inch apart in the other sections. Static taps were located at corresponding locations in the inner wall, except on the rotor hub.

The weight flow was measured by three separate means: (1) An A.S.M.E. orifice with standard radius taps in the 24-inch-diameter downstream piping system. The total pressure and temperature were measured at the upstream, radius tap, station. (2) A total-pressure rake 1.1 inches upstream of the rotor and the inner- and outer-wall static pressure. (3) The survey data at stations 2 and 3.

Station 1 was located 0.10 inch upstream of the rotor. In was instrumented with four static taps approximately 90° apart circumferentially on both the inner wall and outer wall.

PROCEDURE

The compressor rotor was operated at seven speeds from 50 percent to 100 percent of the 1400-foot-per-second design tip speed. The weight-flow range was covered from open throttle to audible surge at each speed. The orifice readings, static pressures, and radial surveys at stations 2 and 3 were taken at each point. The integrated weight flow at stations 2 and 3 was computed as a check on the orifice reading as well as on the survey instruments. Momentum efficiencies were also computed as a check on the survey instruments and thermocouple readings. The blade-element data, mass-weighted total-pressure ratio, and mass-weighted adiabatic and momentum efficiencies were computed as described in reference 22. The performance of the rotor is presented based on the orifice corrected weight flows and the thermocouple temperature readings.

The streamlines, for the blade-element calculations, were assumed to be at radii of equivalent percentage passage height at each station, that is, assuming a linear variation in ρV_z.

ROTOR PERFORMANCE

Average Rotor Performance

The mass-weighted rotor pressure ratio and efficiency based on the survey data taken at station 2 are shown in figures 7 and 8, respectively, plotted against the corrected weight flow based on orifice measurements.

The peak efficiency rotor operating point occurred at 82 percent speed (U_T = 1148 ft/sec) where a rotor efficiency of 94 percent was observed at a pressure ratio of 1.65. At the design speed of 1400 feet per second, the peak efficiency dropped to 89 percent at a rotor pressure ratio of 2.17. Maximum pressure ratio at design speed was 2.21.

The characteristics of the weight-flow range of this rotor compare closely with those of typical subsonic and transonic rotors. There were no apparent discontinuities in pressure ratio between maximum and minimum flow at any speed. The constant weight-flow characteristic associated with design operation of supersonic shock-in-rotor compressors is not obtained, either because of the lower inlet relative Mach number or because the rotor operational characteristics can be expected to be different depending on the type of wave configurations (external or internal) that exist. The maximum weight flow at design speed was below the design value of 30.5 pounds per second.

Radial-Flow Variations

Inlet. - Because of the rotor hub curvature and the required hub fairing section ahead of the rotor, a variation in inlet velocity at the rotor inlet can be expected. The flow variation obtained experimentally is shown in figure 9 compared with the variation assumed in the design. In order to obtain the velocity distribution from wall measurements, a parabolic variation in static pressure between the hub and tip was assumed. The magnitude of the velocity variations at the rotor inlet is seen to be sufficiently large, due to the large hub curvature, as to warrant consideration in the design.

The radial variations of inlet relative Mach number and relative inlet air angle are shown in figures 10 and 11, respectively, for design speed and pressure ratios of 2.2 and 2.0 (points A and C, respectively, of figs. 7 and 8). The design inlet flow angle and the blade mean-line angle are also shown in figure 11. While the variations generally follow the trend used in the design, the magnitudes of both Mach number and relative angle are appreciably different from the design values. The 3° higher incidence angle causes a large reduction in the weight flow from the design value. The change in incidence angle over the weight-flow range is also seen to be less than 1°.

Exit. - The radial variations in outlet flow conditions were obtained from surveys taken at station 2. The radial variations of total-pressure ratio, adiabatic efficiency, absolute outlet Mach number, and absolute outlet angle for speeds of 90 percent, 95 percent, and 100 percent of design are shown in figure 12. Except for the end regions the pressure ratio is seen to be nearly constant across the radius for all speeds with a slightly increasing pressure toward the tip at the maximum-pressure-ratio condition. The efficiency falls off near both ends, with a gradual

reduction along the outer radii starting near the midpassage. The design condition of constant work input is thus not obtained, with larger-than-design work input occurring near the tip and less than design near midpassage. The efficiency drop off near the inner and outer walls with associated reductions in axial velocity results in a gradual rise in outlet air angle toward both rotor hub and tip. For maximum back pressure (point A) at 90 and 95 percent design speed, the effect is most pronounced at the tip and is felt well into the midpassage. At design speed, a marked rise in angle occurs over the outer half of the passage for all pressure ratios.

The Mach numbers entering the stators are slightly higher than conventional for design speed. For 95 percent design speed, the average free-stream Mach number for point B ($P_2/P_1 = 2.03$) is 0.78 and the absolute outlet angle is 40°. If the flow is returned to axial and diffused to the same Mach number as entered the rotor, then the average stator diffusion factor for a tip solidity of 2.0 is 0.45. The losses that might be encountered with stators may be estimated by using the results of reference 24, where a diffusion factor of about 0.45 and an average turning angle of 47° was obtained. At this point, however, the stators of reference 24 appeared to be operating well off the optimum incidence angle for minimum losses. Even if the losses associated with this higher-turning, off-optimum-incidence-angle operation of reference 24 are assumed, the stage pressure ratio of 1.942 at an over-all efficiency of 84 percent would be obtained.

BLADE-ELEMENT PERFORMANCE

The rotor performance is analysed by assuming a blade-element flow as used in reference 22. The blade-element parameters considered were total-pressure loss coefficient, relative Mach number, diffusion factor, deviation angle, axial-velocity ratio, and adiabatic efficiency. These parameters are given as a function of the blade-element incidence angle.

The blade-element parameters are reported at three radial positions, tip, pitch, and hub. The tip and hub sections are taken to be 0.570 inch from the wall at the rotor inlet and 0.340 inch from the wall at the rotor outlet. These sections do not fall within the wall boundary layer as evidenced by the small radial variations in outlet Mach number (fig. 12).

Performance as Function of Incidence Angle

Determination of incidence angle. - The radial static-pressure gradient immediately ahead of the rotor was obtained by assuming a parabolic distribution between the observed inner- and outer-wall static pressures. The small radial velocity component was neglected. Survey data at the

inlet to other rotors tested in the same facility indicated negligible inlet whirl. The inlet air angle was computed by using the axial velocity and the wheel speed. The incidence angle was then obtained from the inlet air angle and the measured blade angle.

Blade-element performance parameters. - The relative total-pressure loss across the rotor was expressed as a ratio of the inlet relative dynamic head $P_1' - p_1$. This ratio $\bar{\omega}$ is computed from equation (B9) of reference 18 with the ideal relative total-pressure ratio of this equation corrected by using the inlet relative stagnation velocity of sound.

The inlet relative Mach number was computed from the axial velocity, the wheel speed, and the velocity of sound determined from the inlet tank total temperature and absolute inlet Mach number. The axial-velocity ratio $V_{z,2}/V_{z,1}$ is the ratio of the axial velocity observed at station 2 to the inlet axial velocity. The adiabatic efficiency η is based on the measured temperature and pressure rise. The deviation angle δ° is based on the measured blade angle, and the computed exit air angle is based on absolute flow measurements.

The diffusion factor D was computed on the assumed streamline by the method utilized in equation (13) of reference 18. The assumptions leading to the velocity distribution used in deriving the diffusion factor may not be strictly applicable in this case because of pressure discontinuities caused by shocks. However, this parameter is useful in comparing the over-all loading of this rotor with that of other rotors; and in the absence of a better criterion, it might still be of use in correlating blade losses.

The computations are based on the data obtained at station 2. The over-all results at station 2 and station 3 generally agreed within 2 percent, 3 percent being the maximum variation in the results between these stations.

Tip performance. - The inlet relative Mach number at the tip section varies from approximately 0.9 to 1.35 for the speed range of 70 percent to 100 percent as shown in figure 13.

The optimum (minimum-loss) incidence angle is nearly constant with speed at a value slightly less than 5°. The total-pressure losses tend to increase and the range of incidence angle for low losses decreases sharply as the speed is increased (fig. 13).

The deviation angle (fig. 13) at 70 percent design speed, where the inlet relative Mach number was less than 1, varied about 2°. The deviation angle for the speeds where the inlet relative Mach number was greater than 1 was nearly constant except for design speed.

The diffusion factors at incidence angles near optimum or minimum-loss points were in the moderate range of values. The diffusion factor increased rapidly with only slight increases in incidence angle at 90 and 100 percent design speed (fig. 13). The adiabatic efficiency followed a trend that was the reverse of the relative total-pressure loss. Maximum values of tip-section element efficiencies of 90 percent or better were observed for all speeds. The axial-velocity ratio (fig. 13) had a minimum value of 1.4 at 70 percent design speed. This high value resulted from the large amount of annular contraction through the rotor and the relatively low pressure ratio at 70 percent design speed. As the speed and pressure ratio increased, the minimum value of the axial-velocity ratio decreased to a value slightly under 1.0 at design speed. Maximum tip element efficiency at design speed occurred at an axial-velocity ratio of about 1.2.

Pitch performance. - The inlet relative Mach number at the pitch section ranged from 0.8 to 1.25. The loss was practically independent of Mach number (fig. 14) and had a rather low value even for the high inlet relative Mach numbers. The optimum incidence angle for design speed appeared slightly higher than the part-speed optimum incidence angles. The trend, however, is not as marked as other investigations have indicated (e.g., ref. 24).

There was little significant trend of deviation angle (fig. 14) other than an increase of slightly over 1° at design speed over the values observed at part speeds.

The diffusion-factor (fig. 14) trend at the pitch section was similar to that at the tip section but at lower values. The efficiency was very high and, in general, remained high over the range of incidence angles encountered (fig. 14).

The axial-velocity-ratio trend (fig. 14) was also similar to that at the tip section. However, at this section, minimum values of axial-velocity ratio occurred near peak efficiency for all speeds. At design-speed peak-efficiency operating point, the axial-velocity ratio was about 1.1.

Hub-section performance. - The inlet relative Mach number range (fig. 15) was from 0.75 to 1.15. The minimum relative total-pressure loss was independent of Mach number. The incidence-angle range again decreased sharply with increased speed. The incidence angle for minimum loss was not sharply defined except at design speed where the loss factor increased rapidly on either side of the minimum-loss incidence angle.

The deviation angle (fig. 15) again increased slightly with increased speeds. At all speeds, near the low-incidence or choked-flow region of operation, the deviation angles increased as back pressure was

reduced. This trend is opposite to that observed for the pitch and tip. A possible explanation is that the hub section chokes and then expands supercritically with a subsequent normal shock. Because of the radial pressure gradient behind the rotor, this tendency for a supersonic expansion followed by a normal shock is greatest at the rotor hub.

The diffusion-factor (fig. 15) trend at the hub again reflected the sensitive relation between incidence angle and loading at the high speeds. Hub-section loading was low for all conditions.

The adiabatic efficiency (fig. 15) decreased very rapidly as choking incidence angles were approached for all but the 70 percent speed. The efficiency peaked at very high values and remained high over most of the range of incidence angles encountered.

The axial-velocity ratio had the same very sharp decrease at the low-incidence-angle range. The peak efficiency at design speed, as for the other sections, occurred at an axial-velocity ratio of about 1.2 (fig. 15).

COMPARISON WITH DESIGN

The design incidence angle was approximately $2\frac{1}{2}^\circ$ while the observed incidence angle at design speed varied from 5° to 6° approximately. An analysis of the blade-passage area indicated that minimum passage area would occur at the exit. Computations of choking incidence angle were made at 82 percent design speed with zero and 8-percent boundary-layer allowance.

The choking incidence angles for 82 percent design speed were 2.1° and 4.9° for zero and 8-percent boundary-layer allowance, respectively. The average inlet relative Mach number was about 1 so that minimum incidence angles would be determined by the choking phenomena. The observed incidence angle of approximately 4° indicates a boundary layer of 6 to 7 percent for the choked-flow condition at 82 percent design speed.

At design speed, the choking incidence angle for an 8-percent boundary layer was 2.4° compared with an average observed angle of 5.1°. For the minimum incidence angle to be determined by choking at the exit, an additional 8 percent for a total boundary-layer blockage of 16 percent would be required. While an increase in boundary-layer thickness at design speed is indicated by the higher deviation angles, the change in deviation angle is not sufficient to account for the required boundary-layer increase. In addition, the change in rotor efficiency does not seem to reflect such a marked change in flow through the rotor.

Because of the supersonic relative velocities existing across the entire blade passage, the possibility exists that the minimum inlet flow angle is determined by a wave pattern as described in reference 1. The computation of this wave pattern is considerably complicated by the three-dimensional nature of the flow, and no attempt was made to determine the wave pattern that might exist ahead of the rotor.

The deviation angle at design speed varied from 4° to 6° as compared with the design deviation angle of about 3°.

The radial variation of work input at design speed is shown in figure 16. The lower pressure-ratio points have nearly a constant work input over the midportion of the passage. The higher pressure-ratio point shows a marked gradient in work input as compared with the constant-work-input design.

The variation of static pressure along the outer casing in the vicinity of the rotor is shown in figure 17. For comparative purposes, the static pressure that would exist for the design mean-velocity distribution with isentropic flow is also shown. The deceleration near the leading edge is obtained for point B. However, for this point the outlet static pressure is appreciably higher than design, indicating diffusion to lower-than-design Mach numbers relative to the blade. This added diffusion was sufficient to overcome the effect of the slightly higher-than-design deviation angle and resulted in a higher-than-design work input. At point C, where nearly design work input was obtained (fig. 16), the start of the deceleration was delayed until well behind the leading edge. While a static-pressure distribution analogous to a spiked diffuser was not obtained at point C, there apparently was sufficient three-dimensional relief to permit a uniform deceleration from the inlet Mach number of 1.35 to slightly below 1.0 without serious shocks or instability.

The static-pressure recovery ψ for point C based on observed pressures just ahead of the rotor and at the rotor trailing edge is 0.34 compared with the design value of 0.31. For point B, the static-pressure recovery had increased to 0.41. The increase in static pressure immediately behind the rotor is probably associated with a reduction in the wake displacement thickness behind the blade. Since the relative outlet Mach numbers are close to 1.0, small changes in the displacement thickness will have an appreciable influence on the Mach number and static-pressure distributions behind the rotor.

CONCLUDING DISCUSSION

The performance obtained from a rotor designed for a 1400-foot-per-second tip speed has indicated that blade-element efficiencies above 90 percent can be obtained at relative Mach numbers up to 1.23 and that rotor

efficiencies approaching 90 percent can be obtained at relative Mach numbers of 1.35. The loss coefficients for the tip section appear to correlate with the diffusion factor, as shown in figure 18(a). The band of data obtained from a large number of conventional rotors and stators shown in reference 18 is also outlined on the figure. The tip-section performance is seen to compare favorably with subsonic and transonic results for speeds up to and including 90 percent (i.e., Mach numbers to 1.23). At design speed ($M_1' = 1.35$) the losses are near the upper limit of the band. The loss levels shown in figures 18(b) and (c) for the pitch and hub sections, respectively, indicate no appreciable deviation from similar plots for subsonic and transonic rotors.

While the derivation of the diffusion factor D was based on incompressible flow, the primary factors influencing performance, that is, over-all diffusion and blade circulation, would not be expected to change for high Mach number applications. The assumed velocity distribution used in the derivation entered only in a very general manner and would have only small influence on the general form of the diffusion-factor relation. However, the empirical constants used in obtaining the correlation with experimental performance will depend on velocity distribution. Thus, the applicability of the correlation of D should be expected only in cases having similar velocity profiles on the blade suction surface. This similarity existed for the theoretical velocity profiles for this rotor, although the actual distribution was probably altered somewhat by differences between the assumed and real flow. On the basis of the comparisons in figure 18, the diffusion factor appears to be a satisfactory loading criterion even for very high Mach number blading when the velocity distribution approximates that of conventional airfoils in cascade.

The axial-velocity ratios for this rotor were 1.15 or greater at the maximum efficiency points. This increase in axial velocity results when the static-pressure diffusion (based on relative velocity head) is distributed equally across the rotor and the stator. Reducing the axial velocity at the rotor discharge would unbalance the diffusion over the two blade rows, thereby loading up the rotor (i.e., increasing D for the rotor). On the basis of the correlations with D shown in figure 18, a design for a reduced outlet axial velocity and the same pressure ratio might well overload the blades to the point of sacrificing efficiency. However, no conclusive data on this point are available for the high level of Mach numbers encountered in this rotor.

The performance of the rotor reported herein compares favorably with that of the transonic type such as reported in references 22, 24, and 25. This performance was obtained with supersonic velocities relative to the rotor across the entire blade span for rotor speeds of 90 percent and above. On the basis of the results of the 1400-foot-per-second rotor, the observation might be made that a subsonic relative Mach number region along the blade span to afford a three-dimensional relief for the sonic and supersonic flow is not required for good efficiencies.

[redacted]

SUMMARY OF RESULTS

Analysis of various design conditions for supersonic compressors indicated possible improvement over previous supersonic compressors if the static-pressure diffusion (expressed as a recovery of the inlet dynamic head) across the stage is proportioned between the rotor and the stator. A supersonic compressor was designed for a tip speed of 1400 feet per second, a pressure ratio of 2.0, and a corrected weight flow of 30.5 pounds per second. The rotor was designed for equal distribution of static-pressure diffusion across the rotor and the stator. Rotor-blade profiles and hub contour were obtained from a channel-flow design approach. Maximum blade thickness was $4\frac{1}{2}$ percent chord.

Over-all performance results of the rotor alone at design speed gave a pressure ratio of 2.17, an adiabatic efficiency of 89 percent, and a weight flow of 28 pounds per second. Maximum efficiency of 94 percent was observed at 82 percent design speed with a pressure ratio of 1.65. Performance characteristics were similar to those of conventional subsonic and transonic rotors with a range in weight flow at good efficiency for all speeds.

Analysis of the blade-element flow through the rotor indicated an angle of incidence at best efficiency of 5° to 6° instead of the design angle of incidence of $2\frac{1}{2}^\circ$. The deviation angle increased slightly at the higher Mach numbers to a value of 4° to 6° as compared with the design deviation of about 3°.

Inlet relative Mach numbers were supersonic across the entire blade span for speeds of 90 percent design and above. Blade-element losses showed no appreciable effect of Mach number for rotor speeds below 90 percent design. At 90 percent design speed and above, an increase in losses at the tip was observed. However, a comparison of blade-element losses based on the rotor diffusion factor showed losses for the higher Mach numbers, that is, up to 1.35, comparable with subsonic and transonic losses at equivalent values of the blade-loading parameters.

The Mach numbers entering the stators are slightly higher than conventional for design speed. For 95 percent design speed and a total-pressure ratio of 2.03, the average free-stream Mach number is 0.78 and the absolute air angle entering the stators is 40°.

Lewis Flight Propulsion Laboratory
National Advisory Committee for Aeronautics
Cleveland, Ohio, January 27, 1955

REFERENCES

1. Kantrowitz, Arthur: The Supersonic Axial-Flow Compressor. NACA Rep. 974, 1950. (Supersedes NACA ACR L6D02.)

2. Wright, Linwood C., and Klapproth, John F.: Performance of Supersonic Axial-Flow Compressors Based on One-Dimensional Analysis. NACA RM E8L10, 1949.

3. Ferri, Antonio: Preliminary Analysis of Axial-Flow Compressors Having Supersonic Velocity at the Entrance to the Stator. NACA RM L9G06, 1949.

4. Wattendorf, Frank L.: High Speed Flow Through Cambered Rotating Grids. Jour. Aero. Sci., vol. 15, no. 4, Apr. 1948, pp. 243-247.

5. Erwin, John R., Wright, Linwood C., and Kantrowitz, Arthur: Investigation of an Experimental Supersonic Axial-Flow Compressor. NACA RM L6J01b, 1946.

6. Johnsen, Irving A., Wright, Linwood C., and Hartmann, Melvin J.: Performance of 24-Inch Supersonic Axial-Flow Compressor in Air. II - Performance of Compressor Rotor at Equivalent Tip Speeds from 800 to 1765 Feet per Second. NACA RM E8G01, 1949.

7. Lown, Harold, and Hartmann, Melvin J.: Investigation of a 24-Inch Shock-in-Rotor Type Supersonic Compressor Designed for Simple Radial Equilibrium Behind Normal Shock. NACA RM E51H08, 1951.

8. Creagh, John W. R., and Klapproth, John F.: Utilization of External-Compression Diffusion Principle in Design of Shock-in-Rotor Supersonic Compressor Blading. NACA RM E53F18, 1953.

9. Jahnsen, Lawrence J., and Hartmann, Melvin J.: Investigation of Supersonic-Compressor Rotors Designed with External Compression. NACA RM E54G27a, 1954.

10. Ullman, Guy N., Hartmann, Melvin J., and Tysl, Edward R.: Experimental Investigation of a 16-Inch Impulse-Type Supersonic-Compressor Rotor. NACA RM E51G19, 1951.

11. Tysl, Edward R., Klapproth, John F., and Hartmann, Melvin J.: Investigation of a Supersonic-Compressor Rotor with Turning to Axial Direction. I - Rotor Design and Performance. NACA RM E53F23, 1953.

12. Goldstein, Arthur W., and Schacht, Ralph L.: Performance of a Supersonic Mixed-Flow Rotor with a Swept Leading Edge and 0.52 Inlet Radius Ratio. NACA RM E53H27, 1953.

[redacted]

13. Klapproth, John F., Ullman, Guy N., and Tysl, Edward R.: Performance of an Impulse-Type Supersonic Compressor with Stators. NACA RM E52B22, 1952.

14. Jacklitch, John J., Jr., and Hartmann, Melvin J.: Investigation of 16-Inch Impulse-type Supersonic Compressor Rotor with Turning Past Axial Direction. NACA RM E53D13, 1953.

15. Hartmann, Melvin J., and Tysl, Edward R.: Investigation of a Supersonic-Compressor Rotor with Turning to Axial Direction. II - Rotor Component Off-Design and Stage Performance. NACA RM E53L24, 1954.

16. Lange, Roy H.: Present Status of Information Relative to the Prediction of Shock-Induced Boundary-Layer Separation. NACA TN 3065, 1954.

17. Nussdorfer, T. J.: Some Observations of Shock-Induced Turbulent Separation on Supersonic Diffusers. NACA RM E51L26, 1954.

18. Lieblein, Seymour, Schwenk, Francis C., and Broderick, Robert L.: Diffusion Factor for Estimating Losses and Limiting Blade Loadings in Axial-Flow-Compressor Blade Elements. NACA RM E53D01, 1953.

19. Stanitz, John D.: Approximate Design Methods for High-Solidity Blade Elements in Compressors and Turbines. NACA TN 2408, 1951.

20. Stanitz, John D., and Prian, Vasily D.: A Rapid Approximate Method for Determining Velocity Distribution on Impeller Blades of Centrifugal Compressors. NACA TN 2421, 1951.

21. Kantrowitz, Arthur, and Donaldson, Coleman DuP.: Preliminary Investigation of Supersonic Diffusers. NACA WR-713, 1945. (Supersedes NACA ACR L5D20.)

22. Schwenk, Francis C., Lieblein, Seymour, and Lewis, George W., Jr.: Experimental Investigation of an Axial-Flow Compressor Inlet Stage Operating at Transonic Relative Inlet Mach Numbers. III - Blade-Row Performance of Stage with Transonic Rotor and Subsonic Stator at Corrected Tip Speeds of 800 and 1000 Feet Per Second. NACA RM E53G17, 1953.

23. NACA Subcommittee on Compressors: Standard Procedures for Rating and Testing Multistage Axial-Flow Compressors. NACA TN 1138, 1946.

[redacted]

24. Sandercock, Donald M., Lieblein, Seymour, and Schwenk, Francis C.: Experimental Investigation of an Axial-Flow Compressor Inlet Stage Operating at Transonic Relative Inlet Mach Numbers. IV - Stage and Blade-Row Performance of Stage with Axial-Discharge Stators. NACA RM E54C26, 1954.

25. Tysl, Edward R., Schwenk, Francis C., and Watkins, Thomas B.: Experimental Investigation of a Transonic Compressor Rotor with a 1.5-Inch-Chord Length and an Aspect Ratio of 3.0. I - Design, Over-All Performance, and Rotating-Stall Characteristics. NACA RM E54L31, 1955.

[redacted]

TABLE I. - BLADE AND HUB COORDINATES[a]

X	SECTION										r_h
	B-B		C-C		D-D		E-E		F-F		
	Y_U	Y_L	Y_U	Y_L	Y_U	Y_L	Y_U	Y_L	Y_U	Y_L	
0	-1.206	-1.206	-1.229	-1.229	-1.284	-1.284	-1.367	-1.367	-1.434	-1.434	5.600
.20	-0.840	-0.950	-0.872	-0.988	-0.956	-1.050	-1.060	-1.148	-1.133	-1.220	5.651
.40	-0.486	-0.667	-0.544	-0.717	-0.630	-0.788	-0.750	-0.905	-0.837	-0.981	5.710
.60	-0.146	-0.378	-0.224	-0.445	-0.317	-0.527	-0.454	-0.656	-0.551	-0.746	5.783
.80	0.157	-0.092	0.070	-0.178	-0.026	-0.273	-0.177	-0.407	-0.283	-0.513	5.871
1.00	0.430	0.189	0.339	0.085	0.230	-0.024	0.080	-0.169	-0.037	-0.290	5.965
1.20	0.668	0.466	0.576	0.342	0.458	0.216	0.313	0.067	0.185	-0.070	6.066
1.40	0.881	0.722	0.784	0.584	0.657	0.445	0.507	0.284	0.365	0.132	6.172
1.60	1.084	0.957	0.967	0.804	0.836	0.656	0.675	0.480	0.523	0.319	6.274
1.80	1.269	1.180	1.130	1.005	0.996	0.851	0.823	0.653	0.663	0.491	6.370
1.996	1.400	1.400	-----	-----	-----	-----	-----	-----	-----	-----	-----
2.00	-----	-----	1.279	1.188	1.138	1.025	0.951	0.816	0.783	0.641	6.458
2.20	-----	-----	1.417	1.362	1.257	1.180	1.060	0.960	0.884	0.767	6.528
2.258	-----	-----	1.423	1.423	-----	-----	-----	-----	-----	-----	-----
2.40	-----	-----	-----	-----	1.370	1.320	1.149	1.078	0.963	0.870	6.567
2.433	-----	-----	-----	-----	1.355	1.355	-----	-----	-----	-----	-----
2.48	-----	-----	-----	-----	-----	-----	-----	-----	-----	-----	6.570
2.60	-----	-----	-----	-----	-----	-----	1.223	1.175	1.020	0.951	6.570
2.658	-----	-----	-----	-----	-----	-----	1.214	1.214	-----	-----	6.570
2.806	-----	-----	-----	-----	-----	-----	-----	-----	1.035	1.035	6.570
3.188	-----	-----	-----	-----	-----	-----	-----	-----	-----	-----	6.570

[a]Dimensions are in inches; sections and their notation are defined in fig. 5(a).

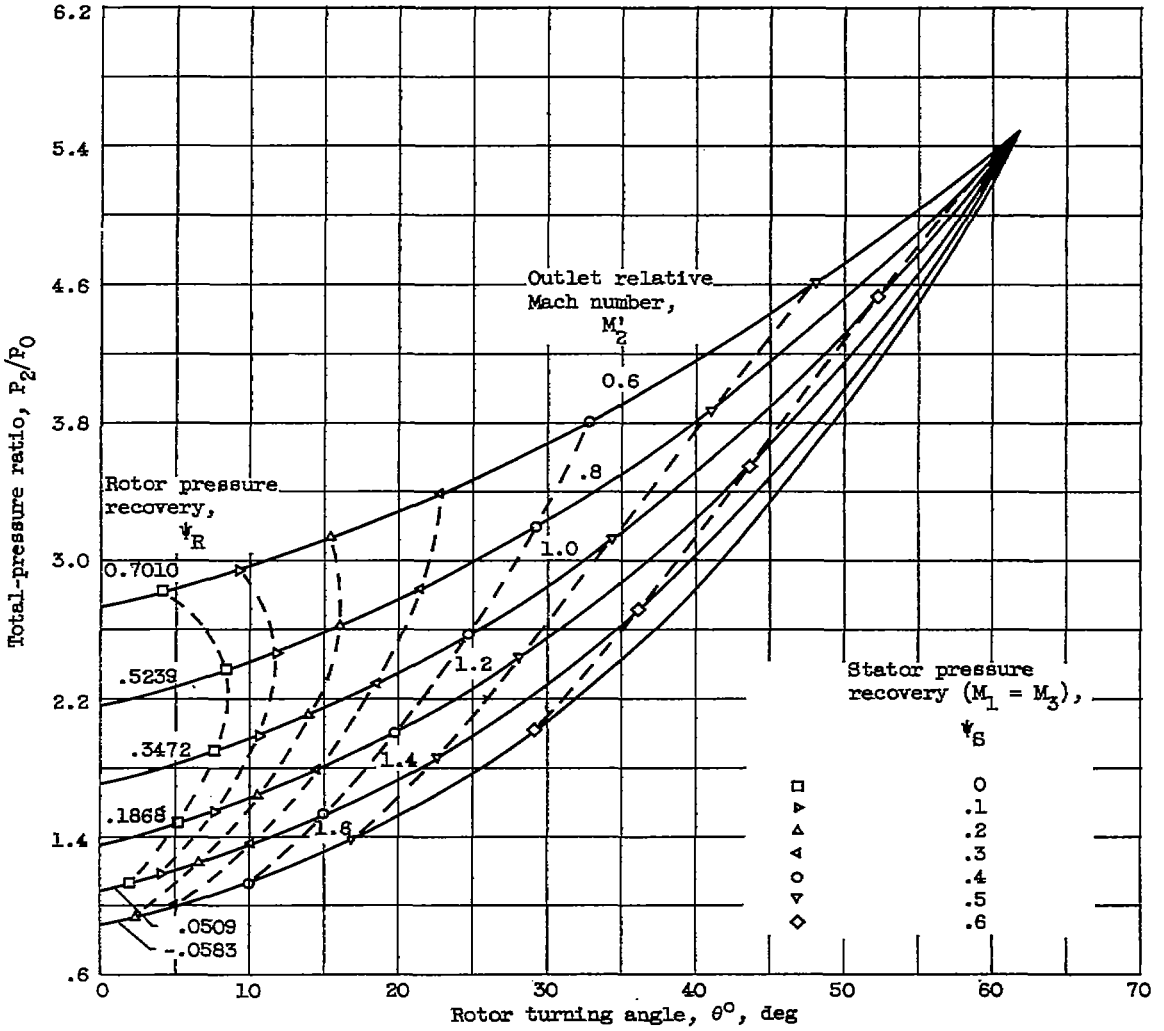

(a) Rotational speed, 1400 feet per second.

Figure 1. - Isentropic total-pressure ratio as function of rotor and stator diffusion.

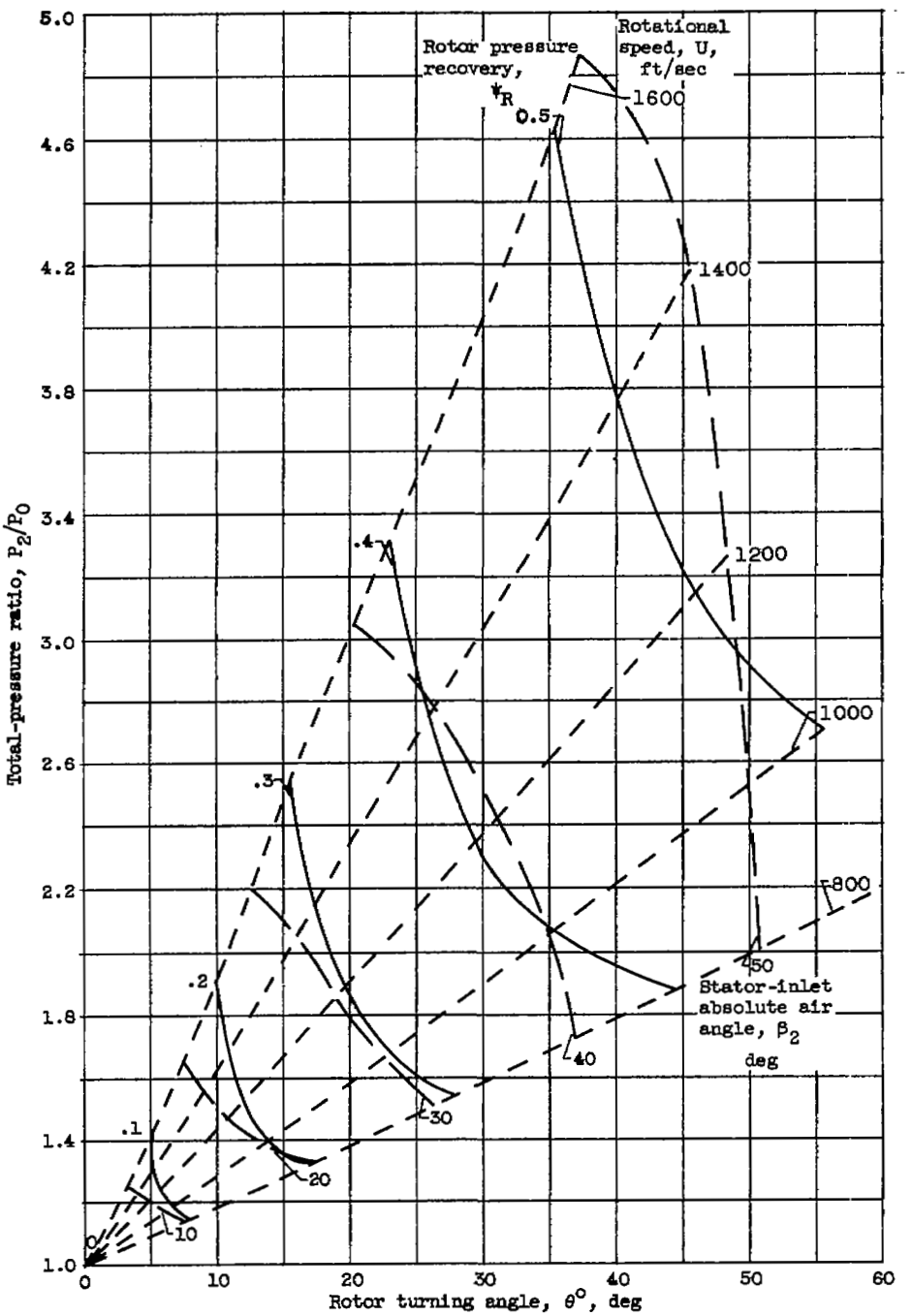

(b) Equal diffusion in rotor and stator ($\psi_R = \psi_S$).

Figure 1. - Concluded. Isentropic total-pressure ratio as function of rotor and stator diffusion.

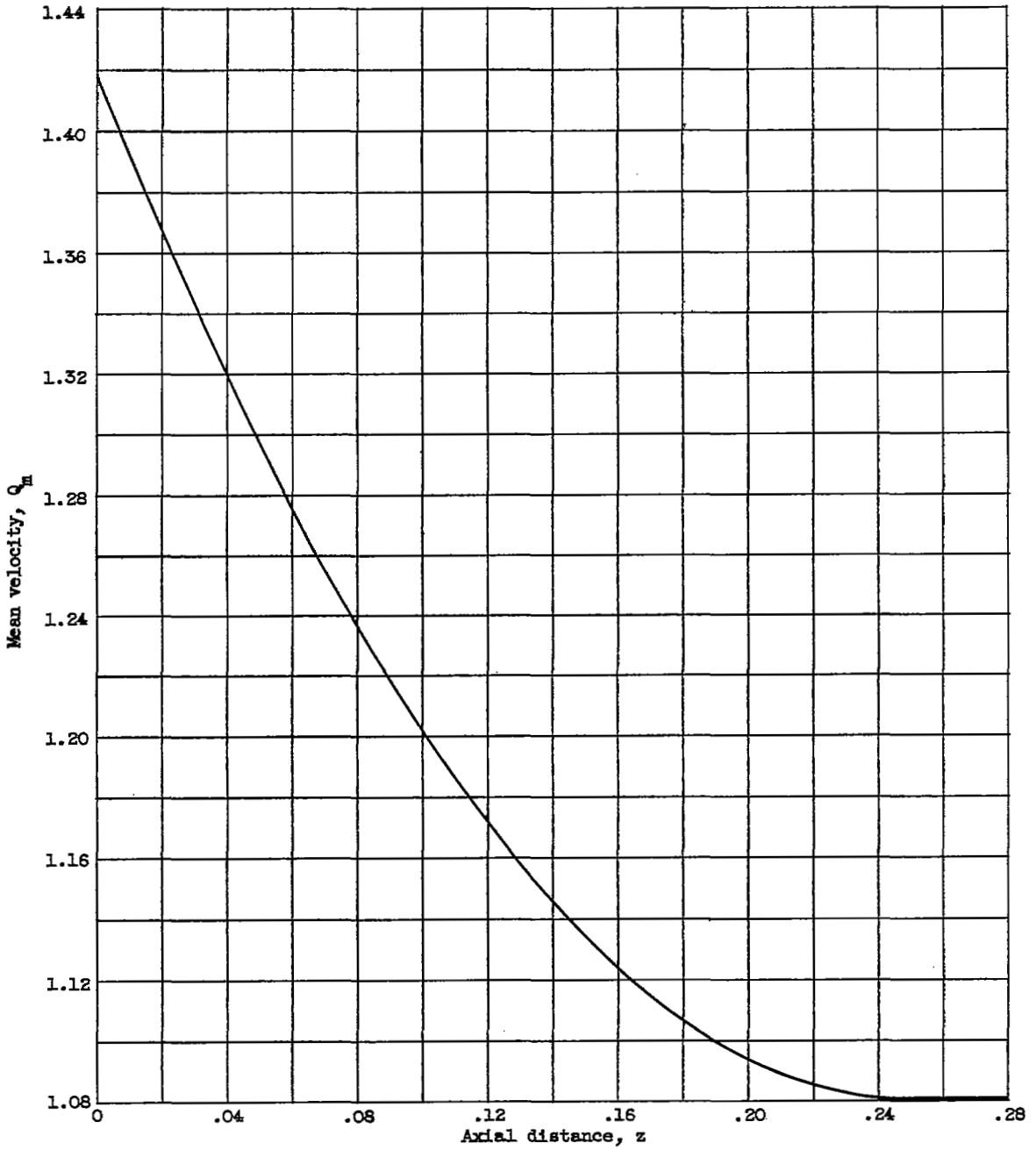

(a) Mean velocity for tip section.

Figure 2. - Blade design parameters.

[redacted]

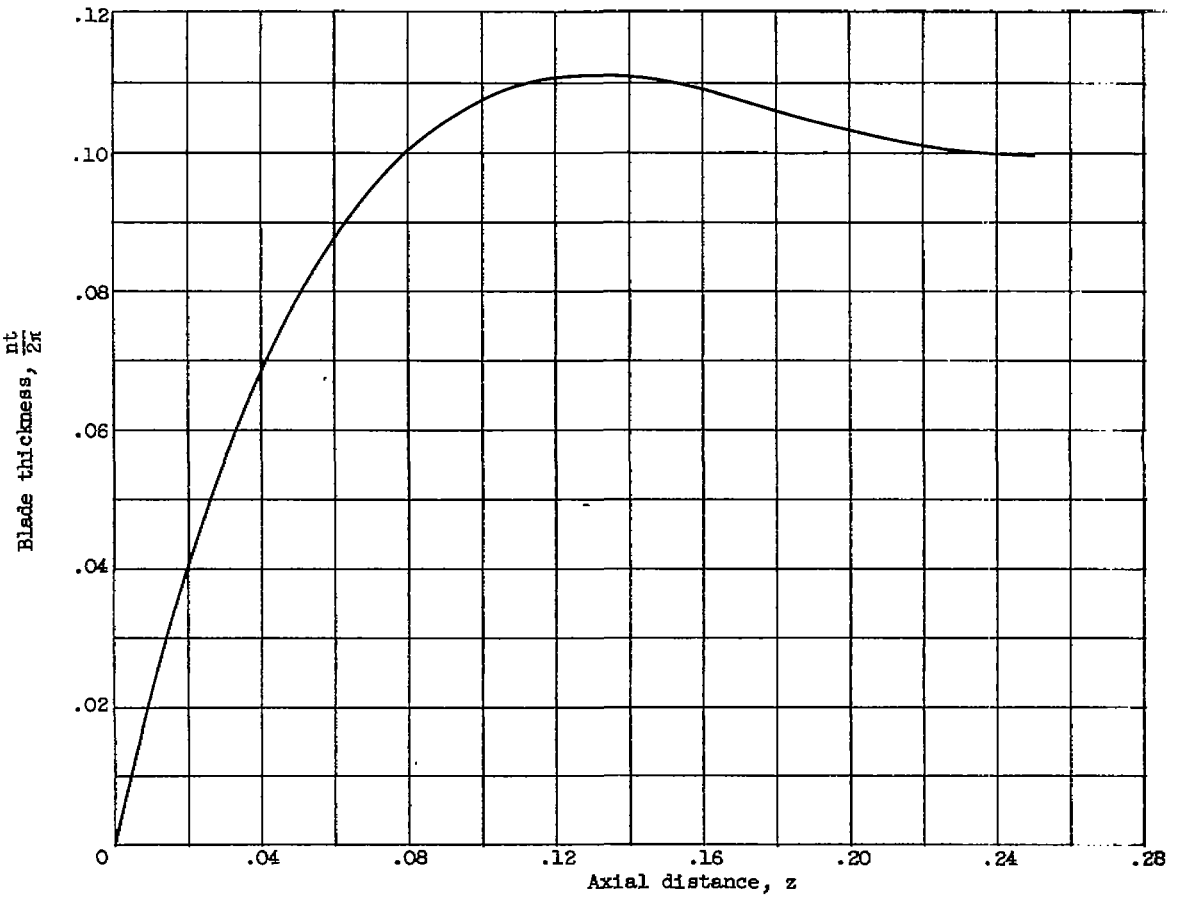

(b) Thickness for all sections.

Figure 2. - Continued. Blade design parameters.

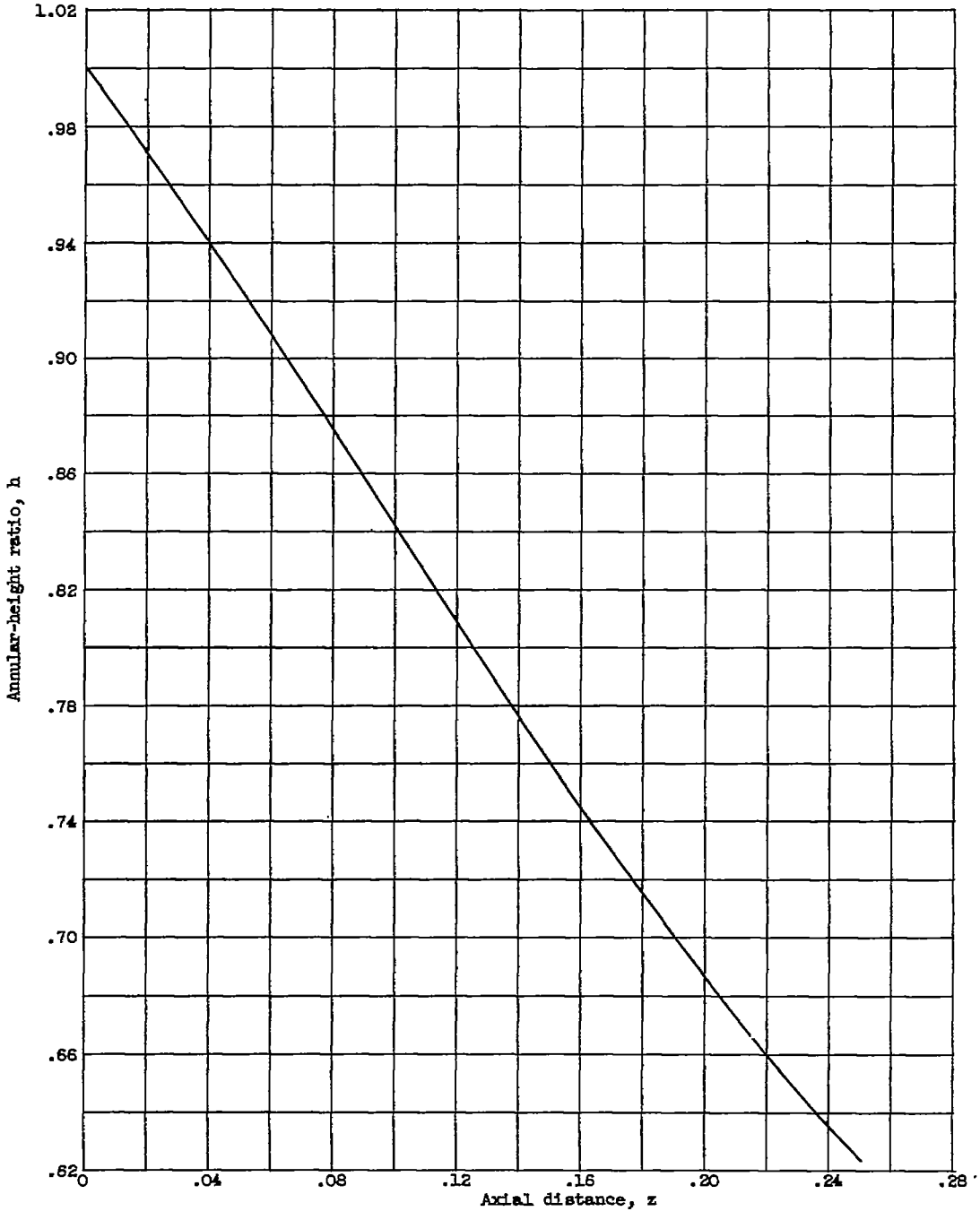

(c) Annular height for tip section.

Figure 2. - Concluded. Blade design parameters.

[redacted]

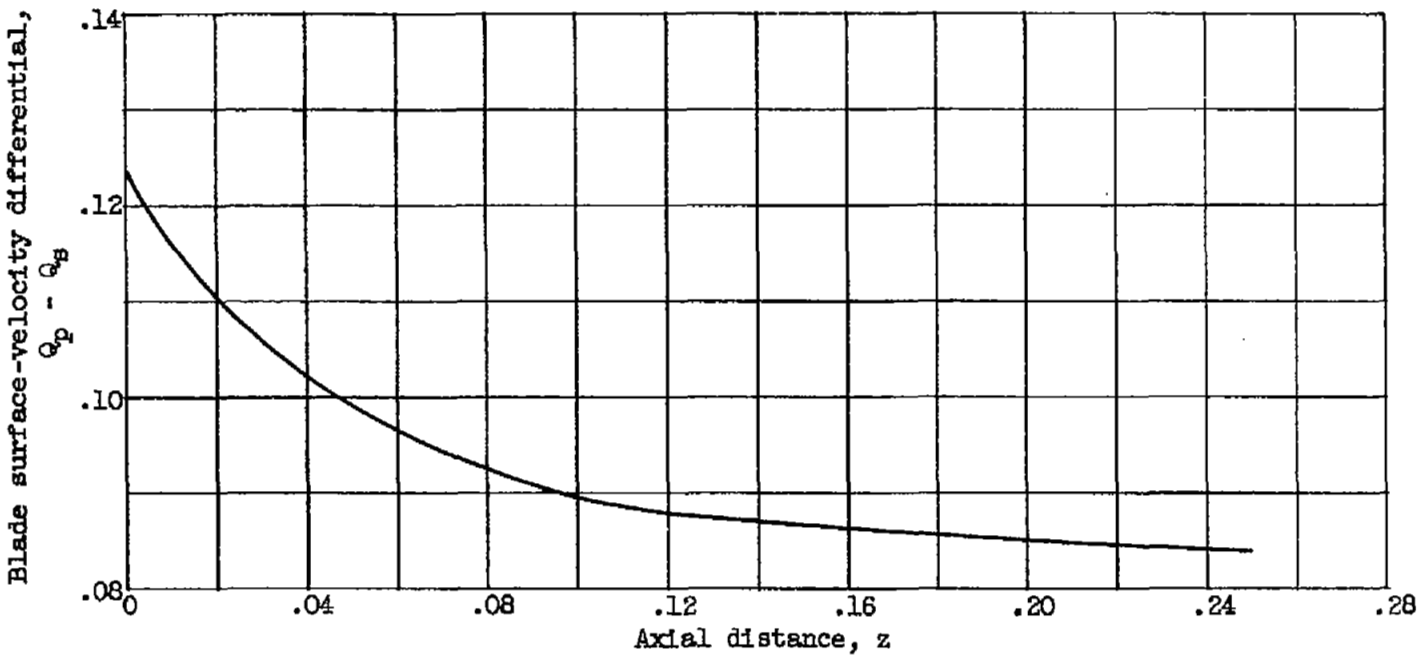

Figure 3. - Blade loading.

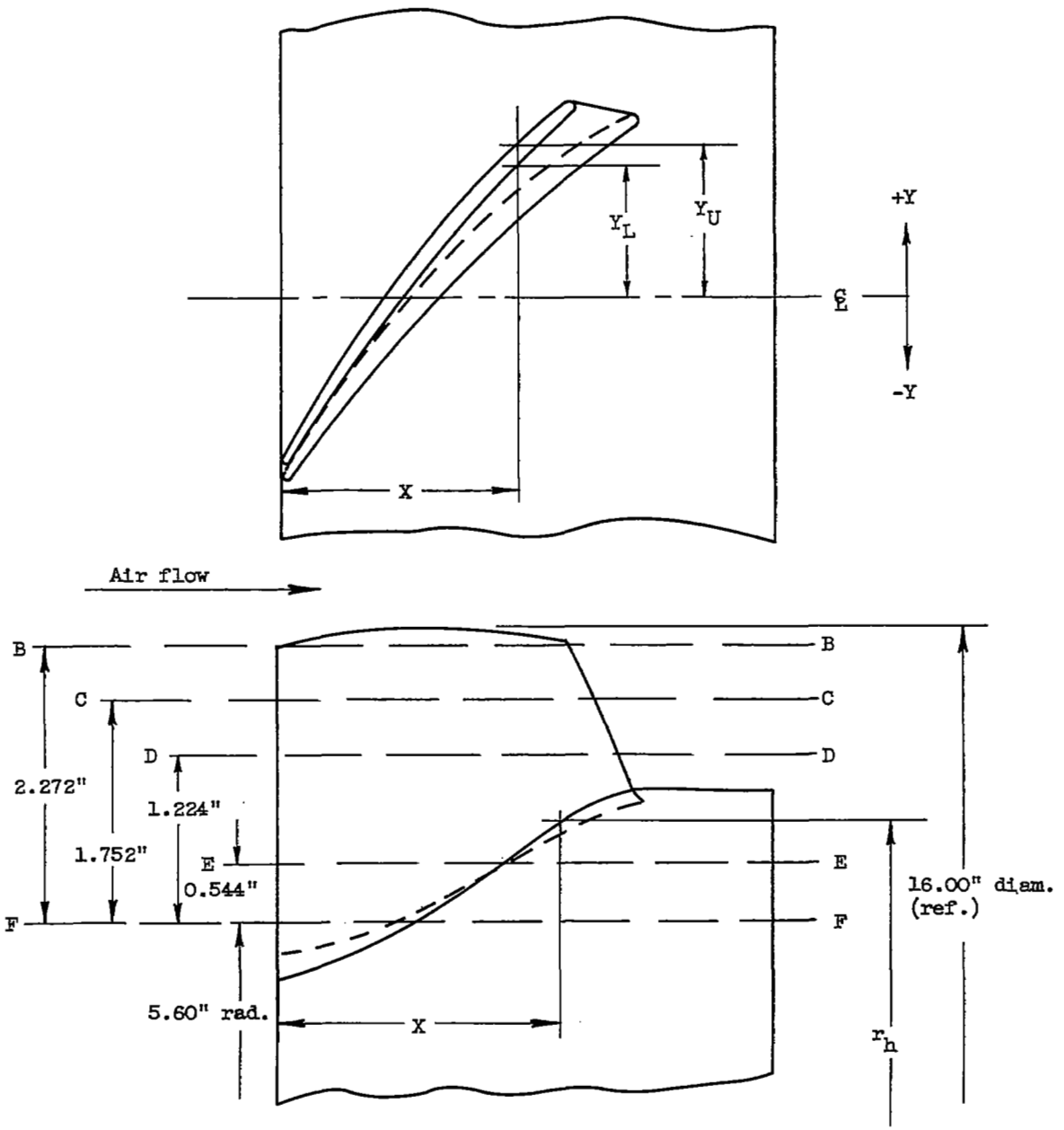

Figure 4. - Rotor-blade shape and definition of coordinates.

Figure 5. - Supersonic compressor rotor designed for tip speed of 1400 feet per second.

Figure 6. - Schematic diagram of supersonic-compressor test rig.

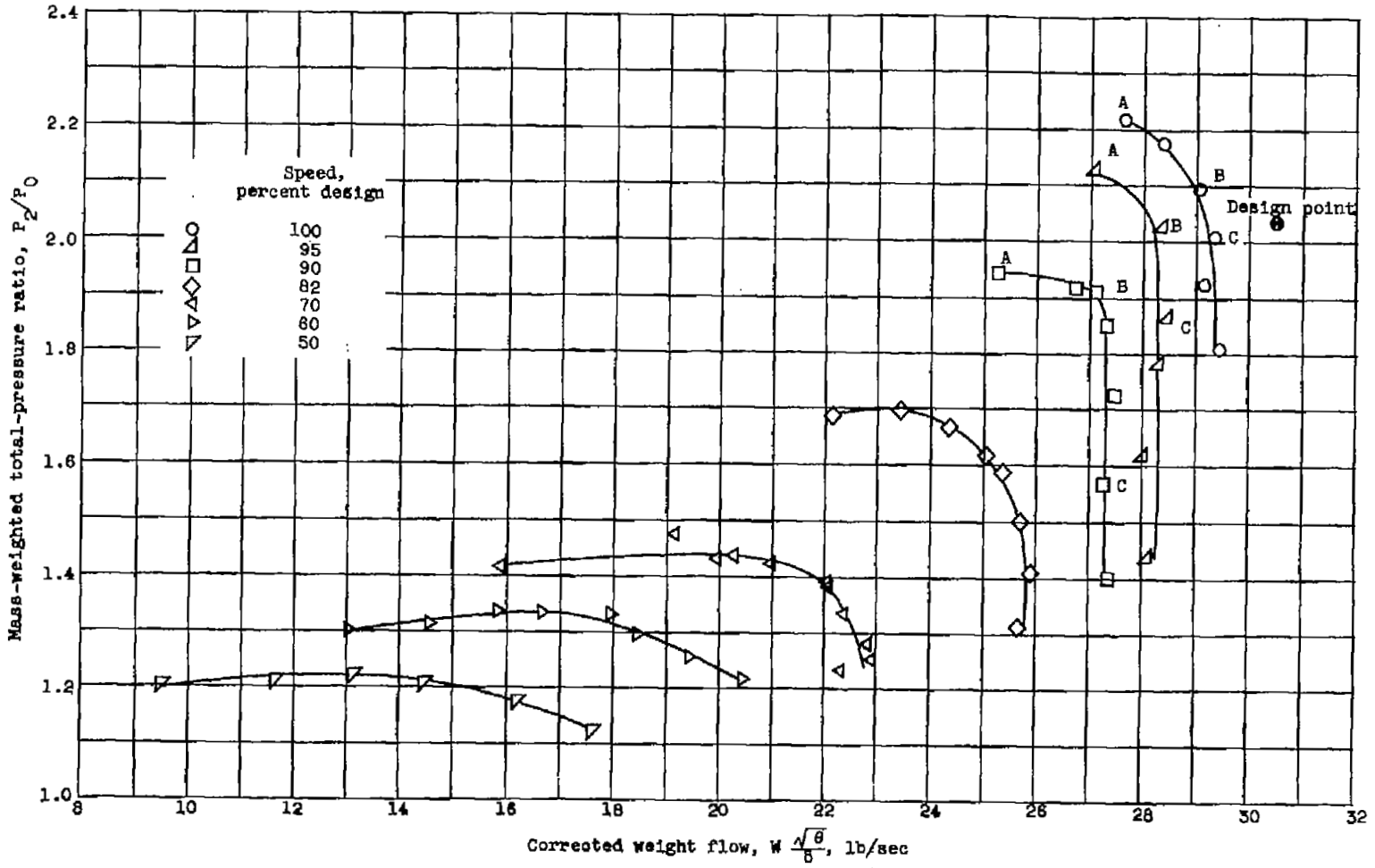

Figure 7. - Mass-weighted total-pressure ratio.

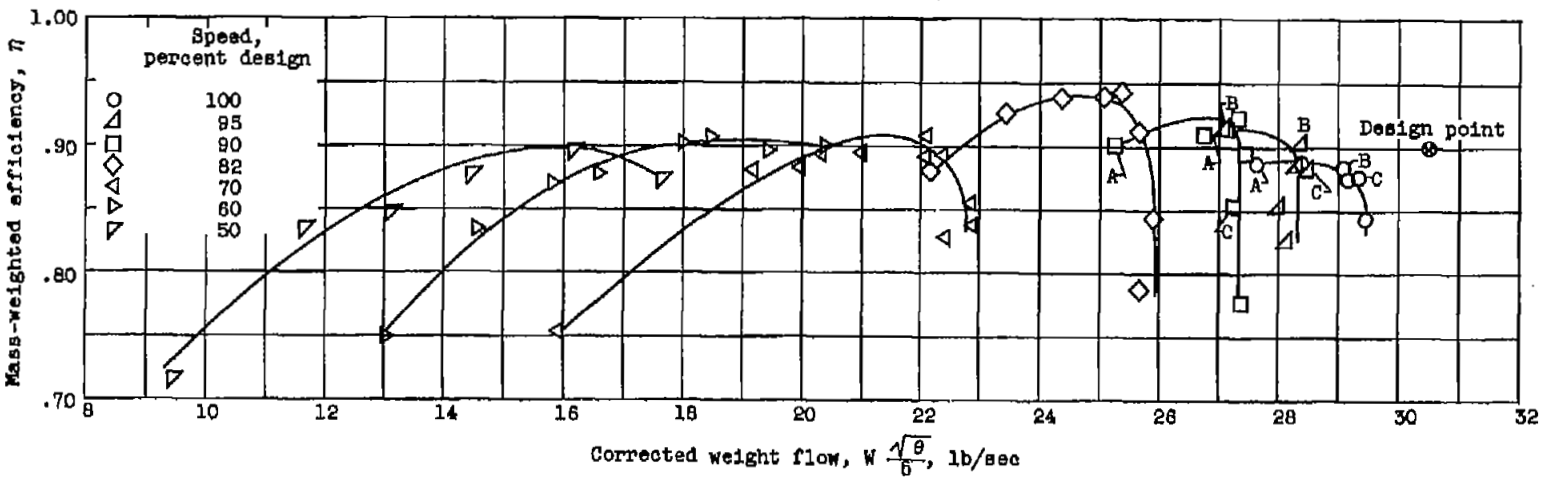

Figure 8. - Mass-weighted adiabatic efficiency.

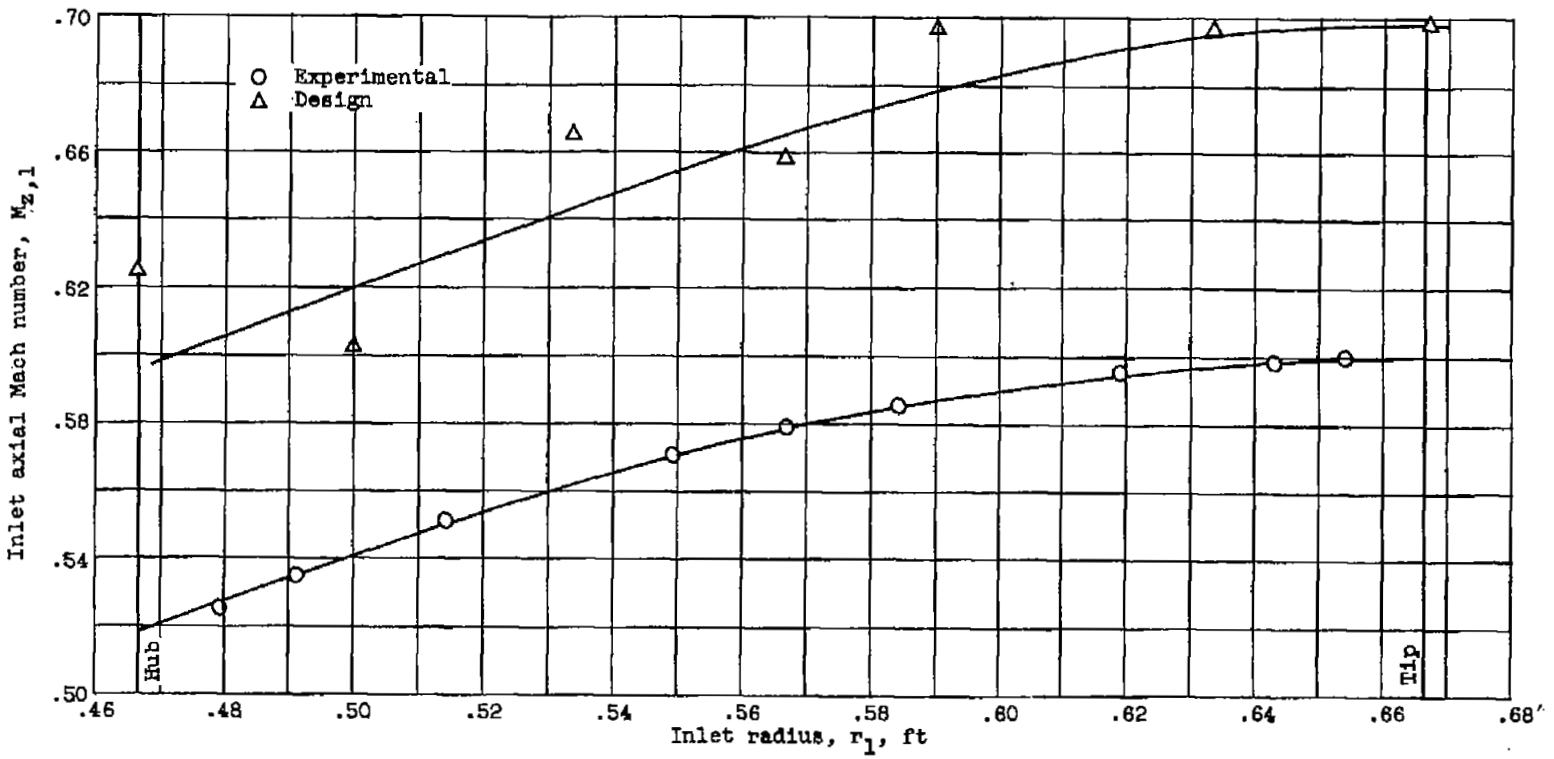

Figure 9. - Radial variation of inlet axial Mach number at design speed.

Figure 10. - Radial variation of experimental inlet relative Mach number at design speed.

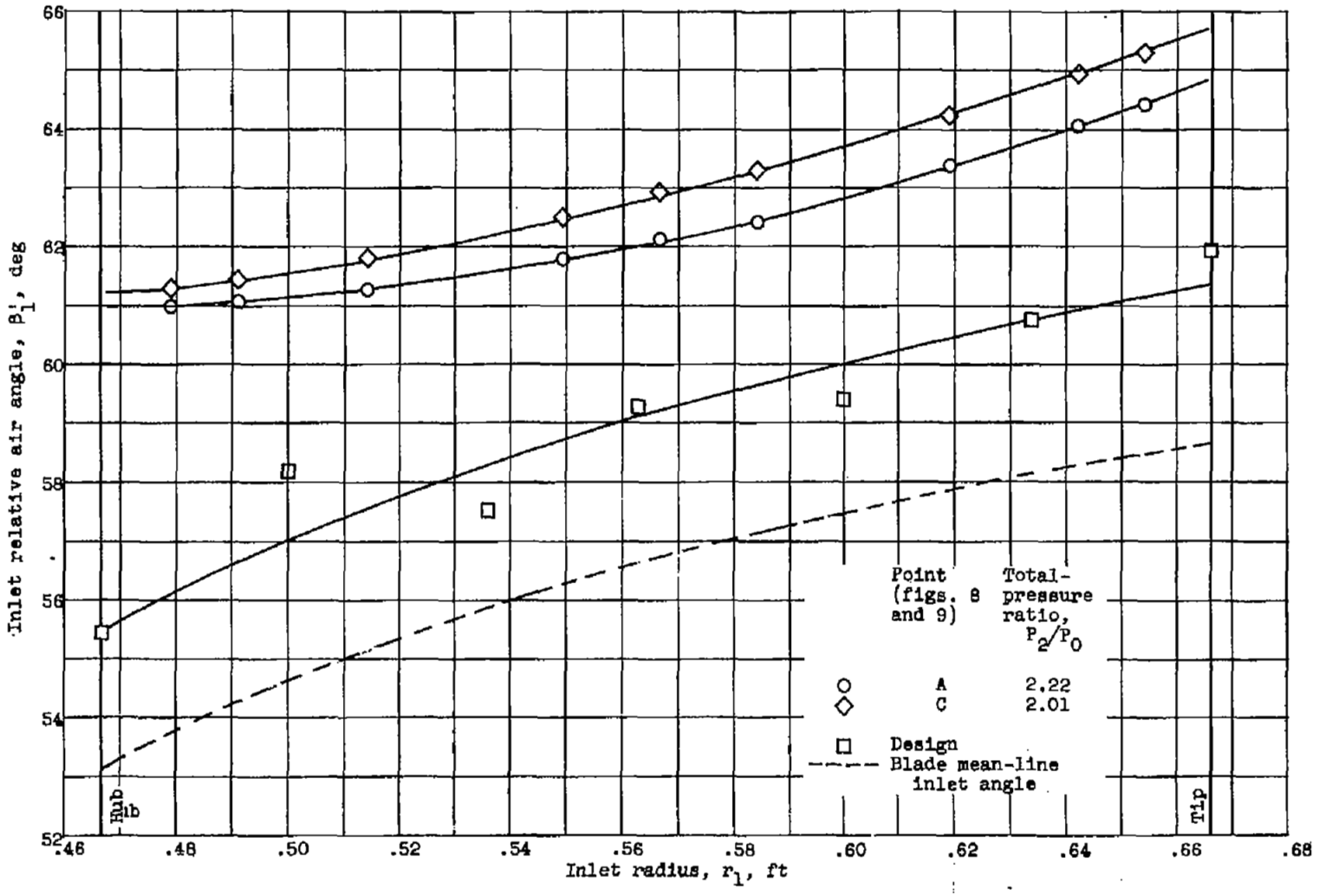

Figure 11. - Radial variation of experimental inlet relative air angle at design speed.

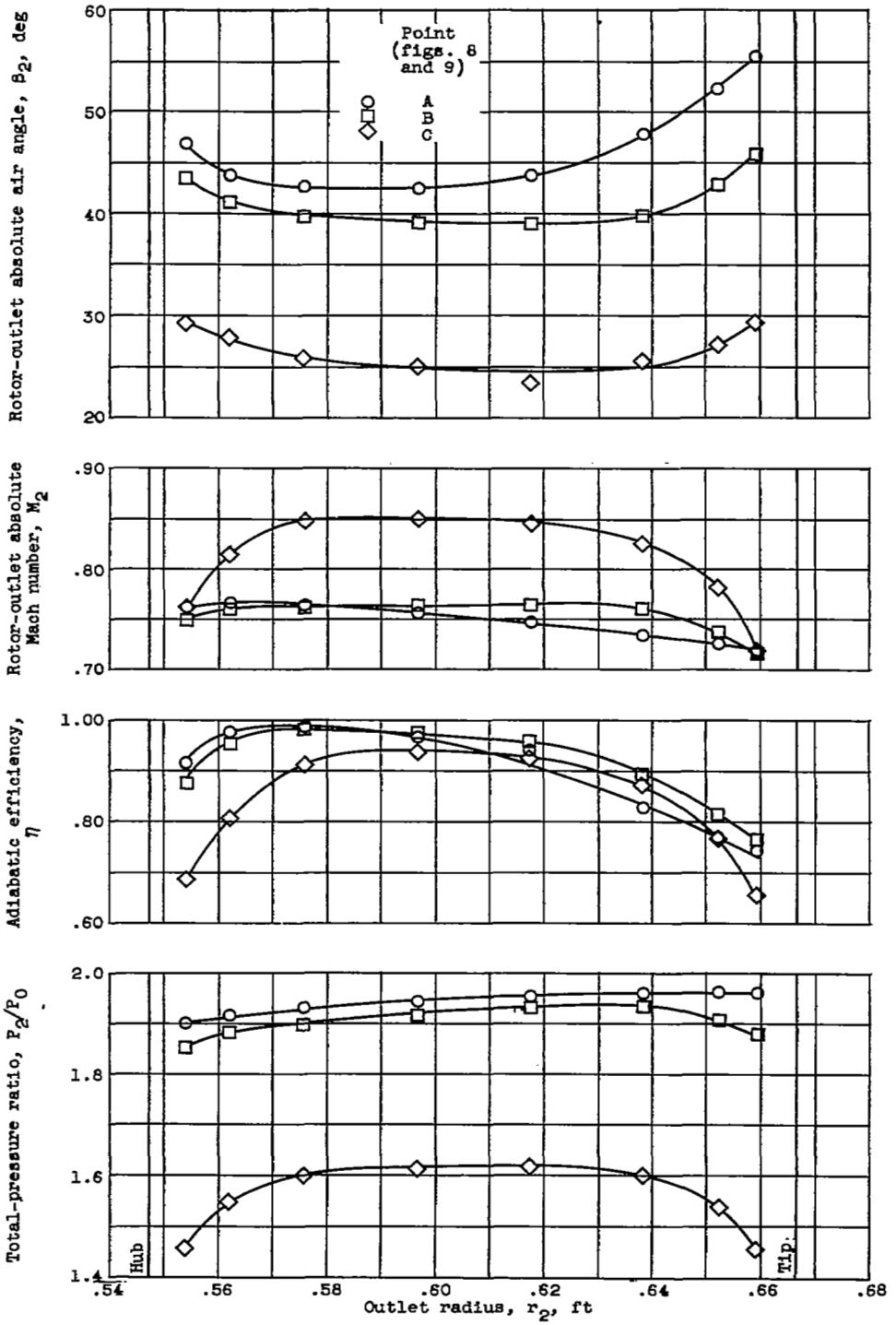

(a) 90 Percent design speed.

Figure 12. - Radial variation of outlet conditions.

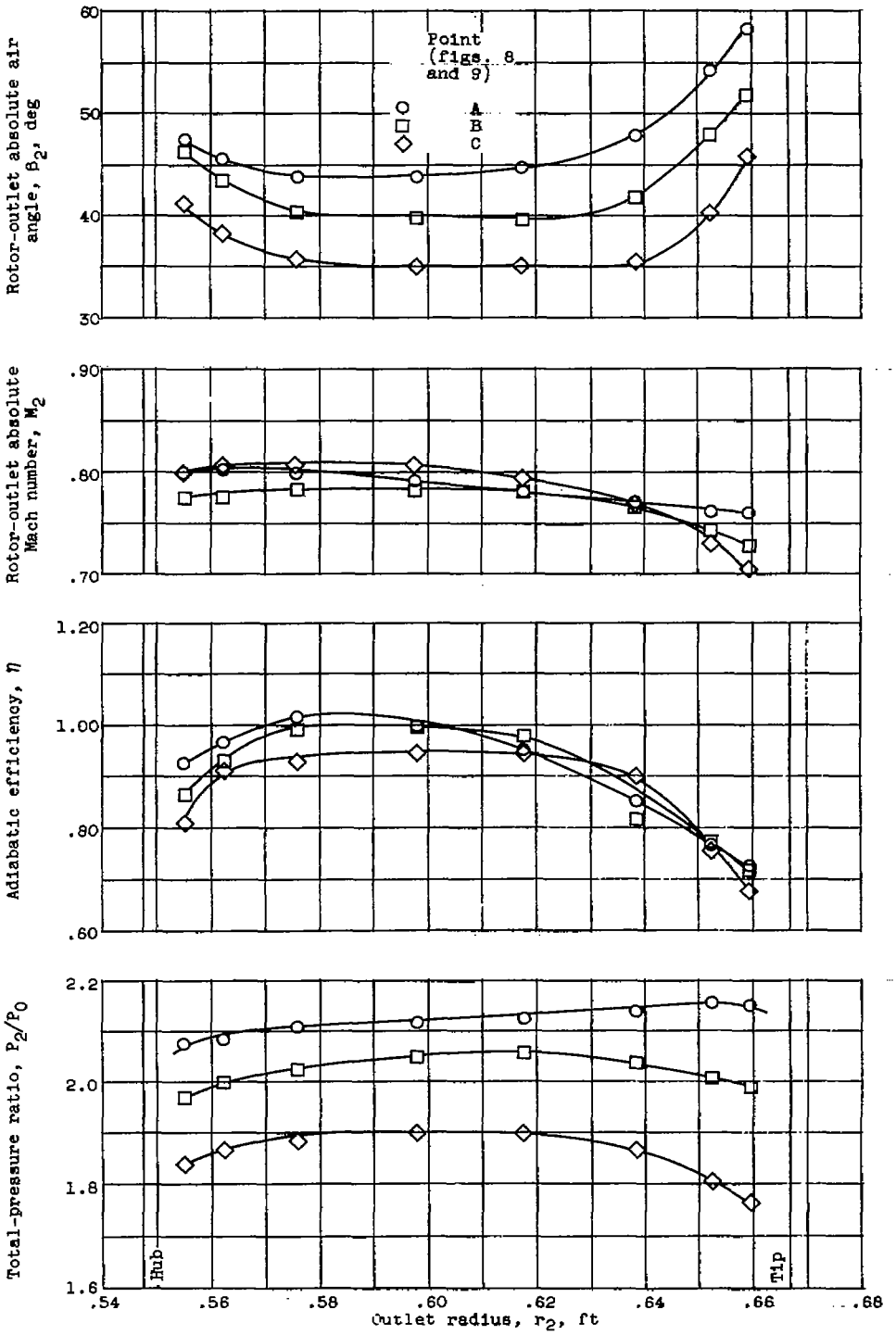

(b) 95 Percent design speed.

Figure 12. - Continued. Radial variation of outlet conditions.

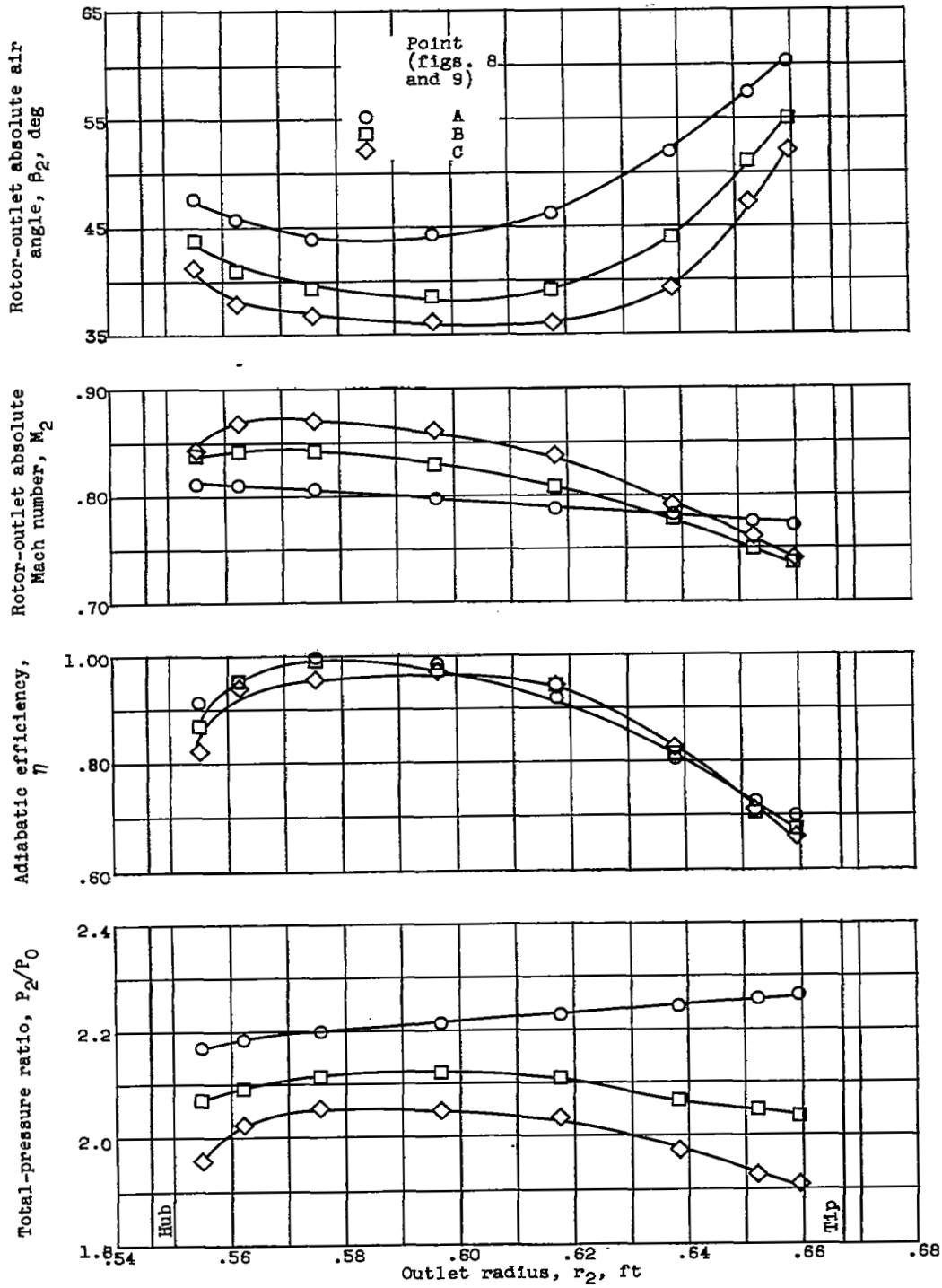

(c) Design speed.

Figure 12. - Concluded. Radial variation of outlet conditions.

[redacted]

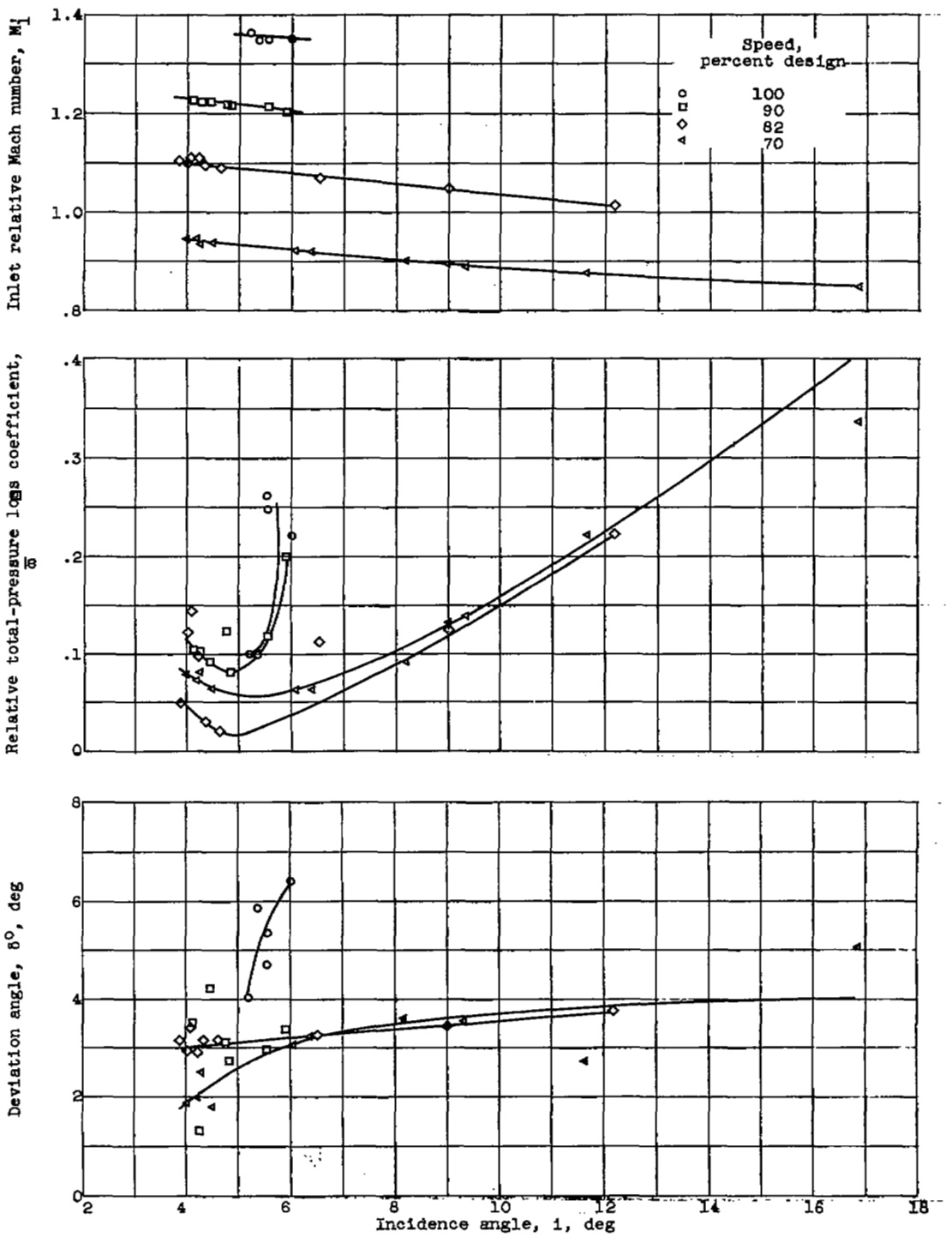

Figure 13. - Tip-section blade-element characteristics.

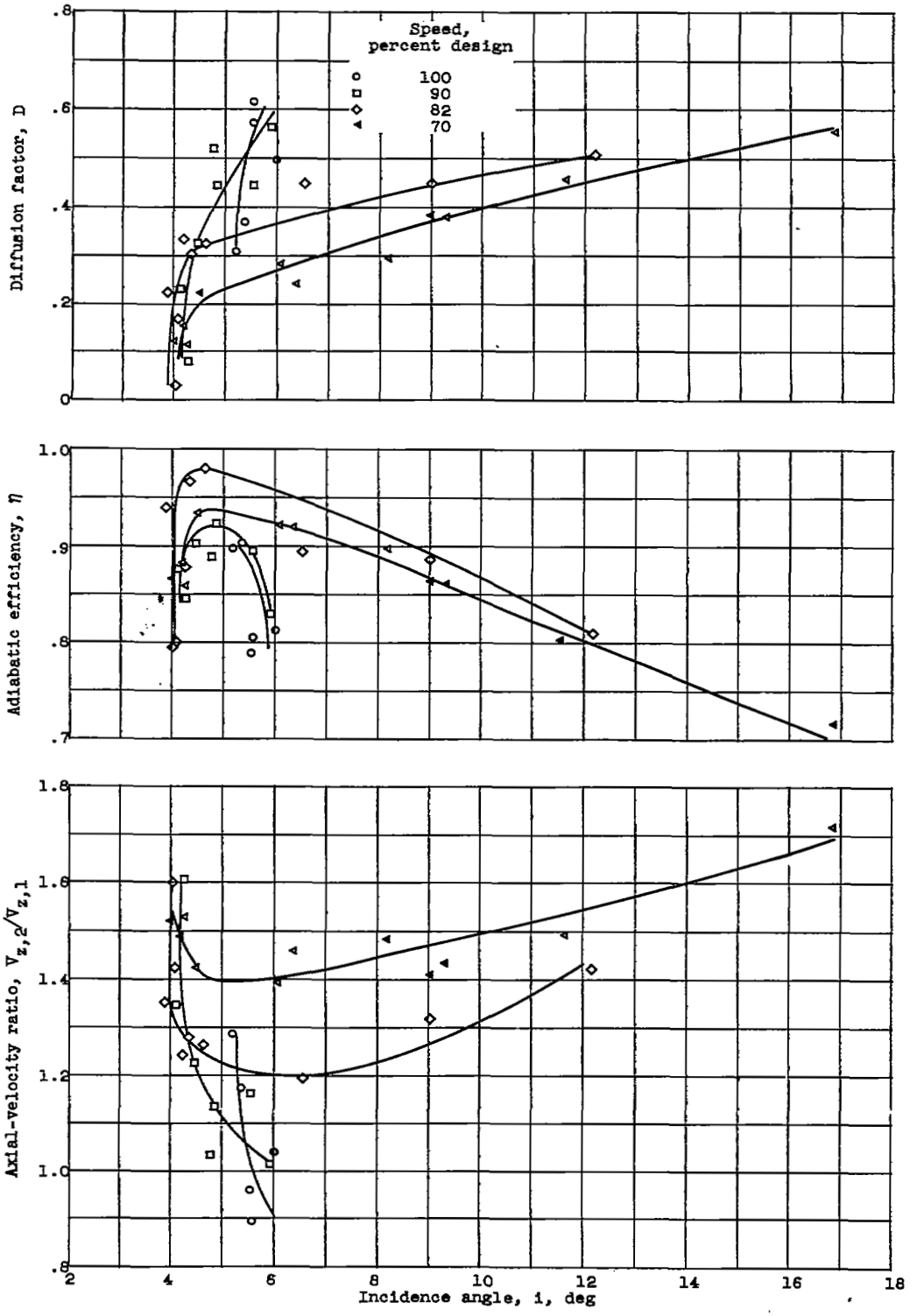

Figure 13. - Concluded. Tip-section blade-element characteristics.

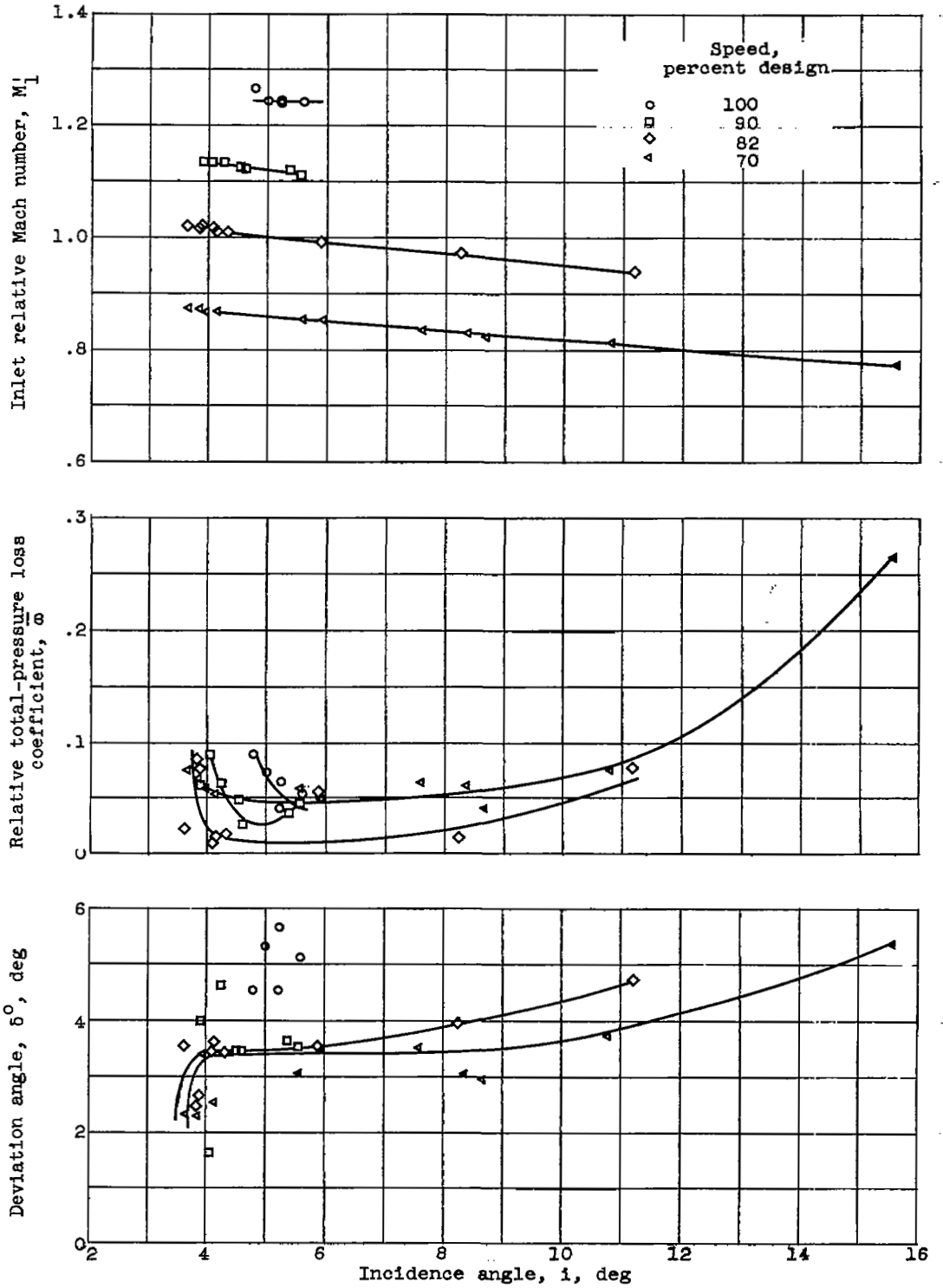

Figure 14. - Pitch-section blade-element characteristics.

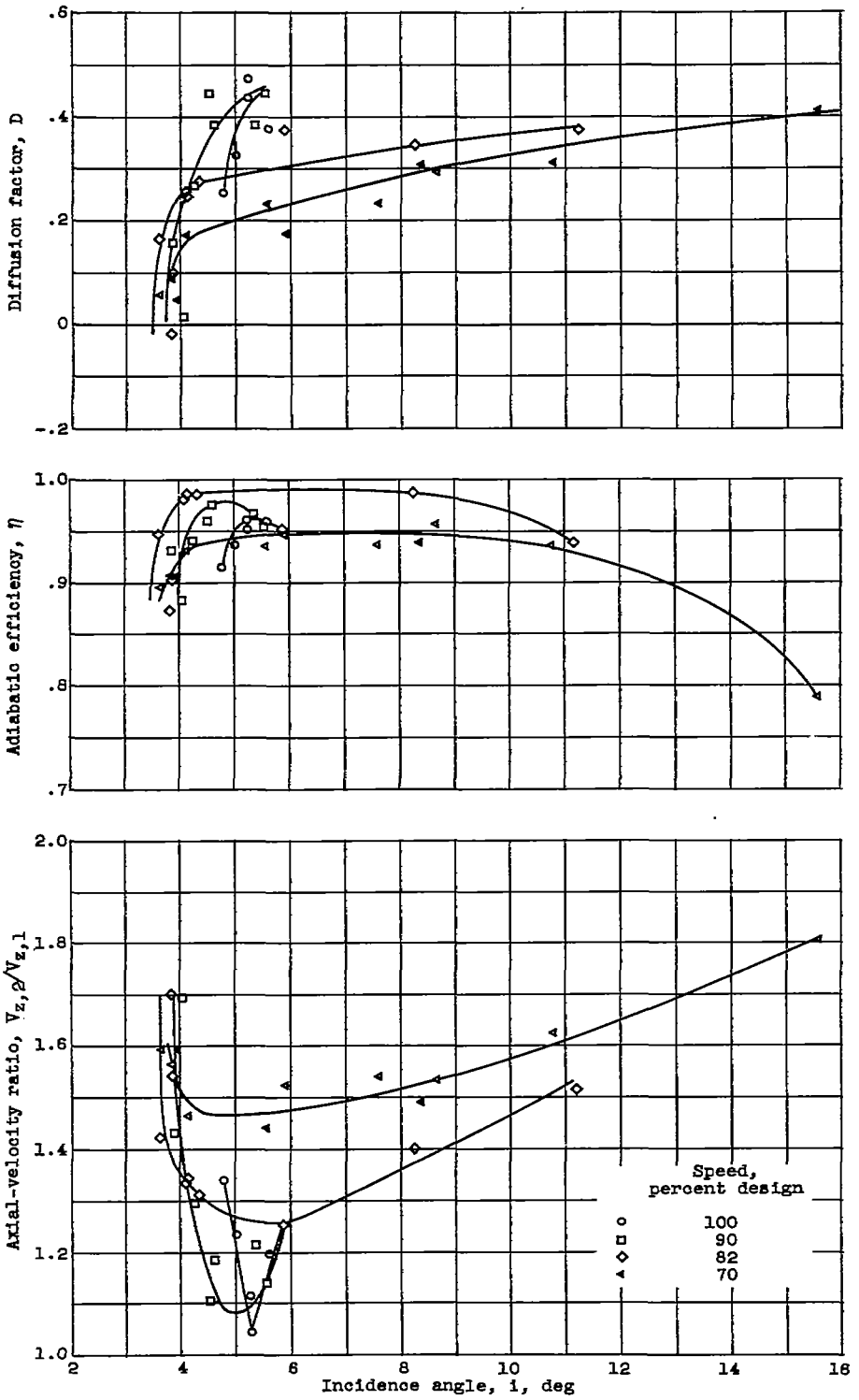

Figure 14. - Concluded. Pitch-section blade-element characteristics.

[redacted]

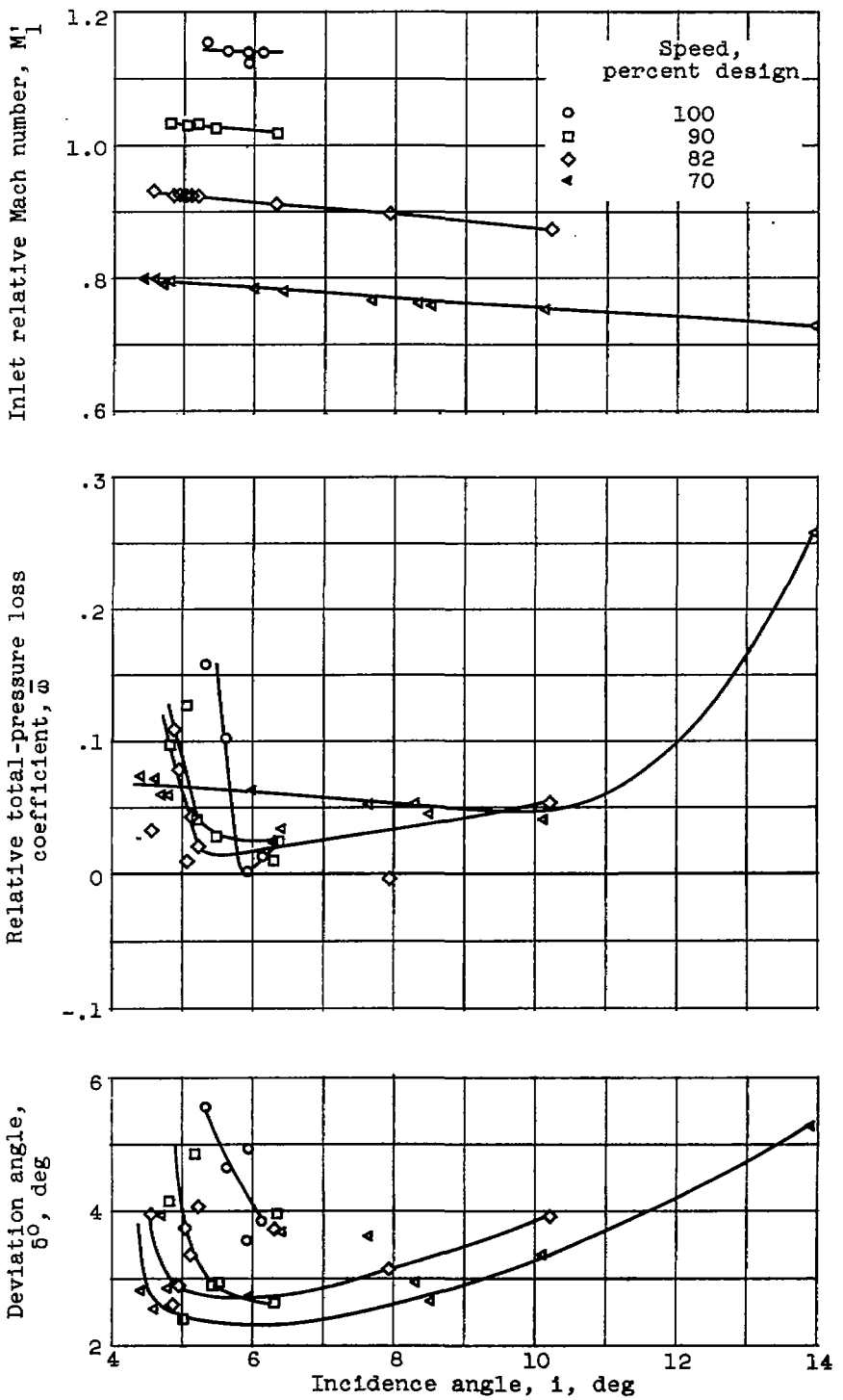

Figure 15. - Hub-section blade-element characteristics.

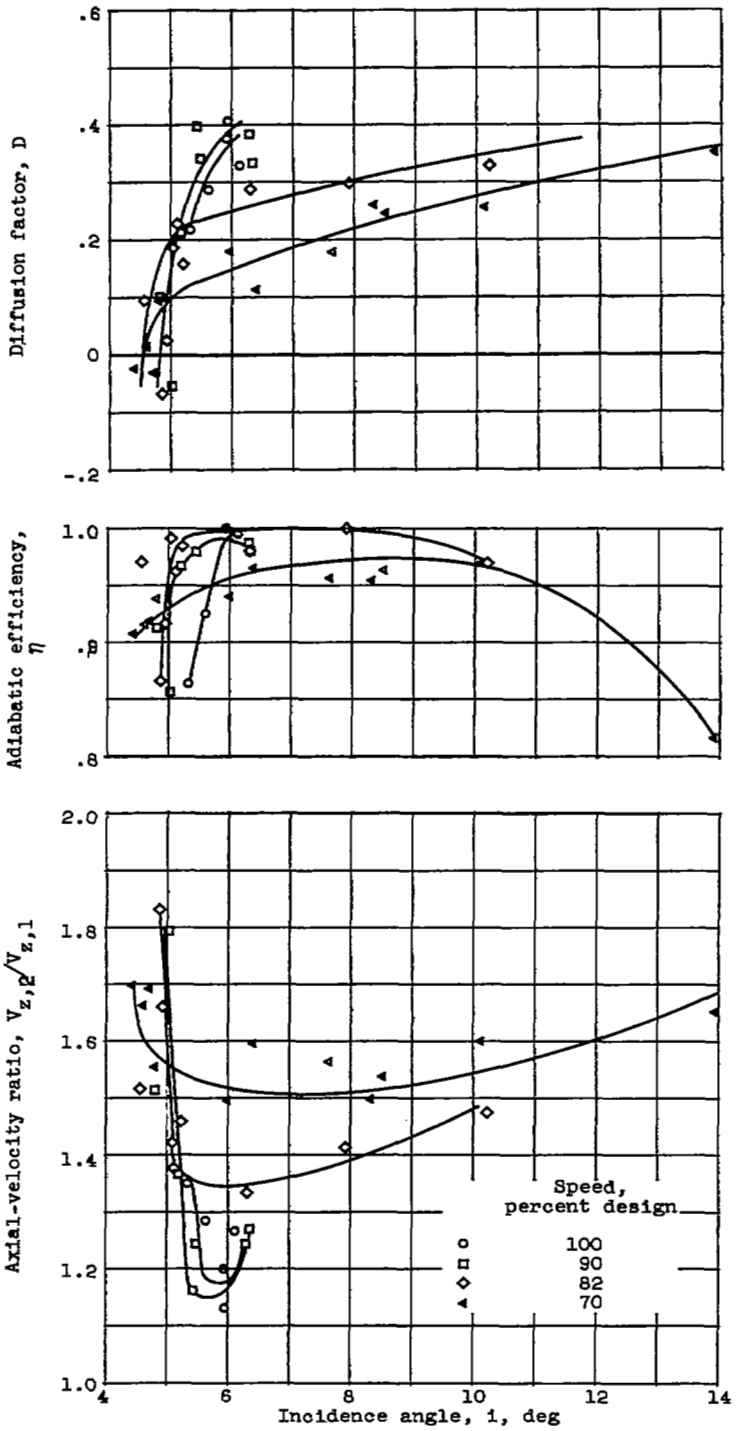

Figure 15. - Concluded. Hub-section blade-element characteristics.

[redacted]

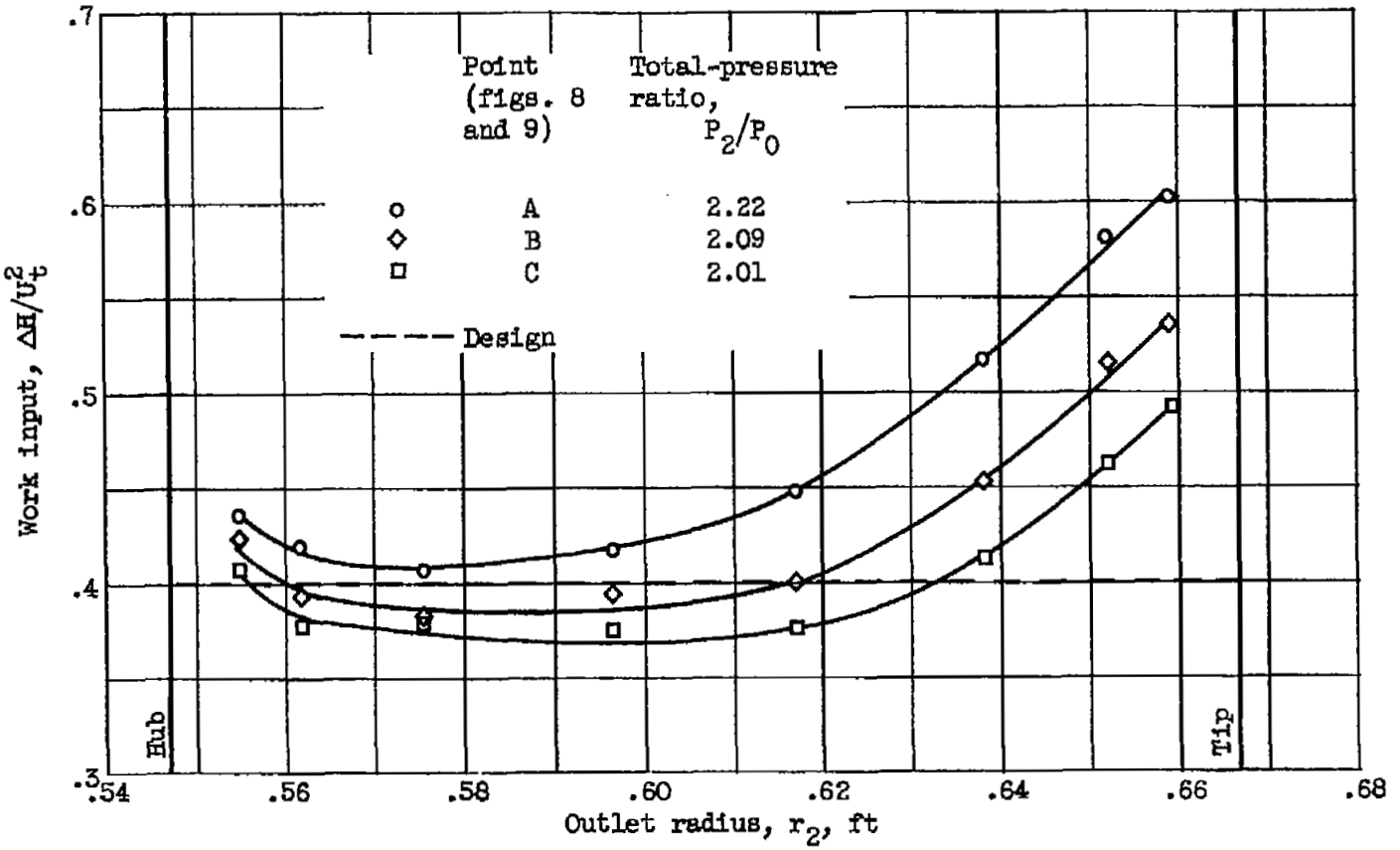

Figure 16. - Radial variation of work input at design speed.

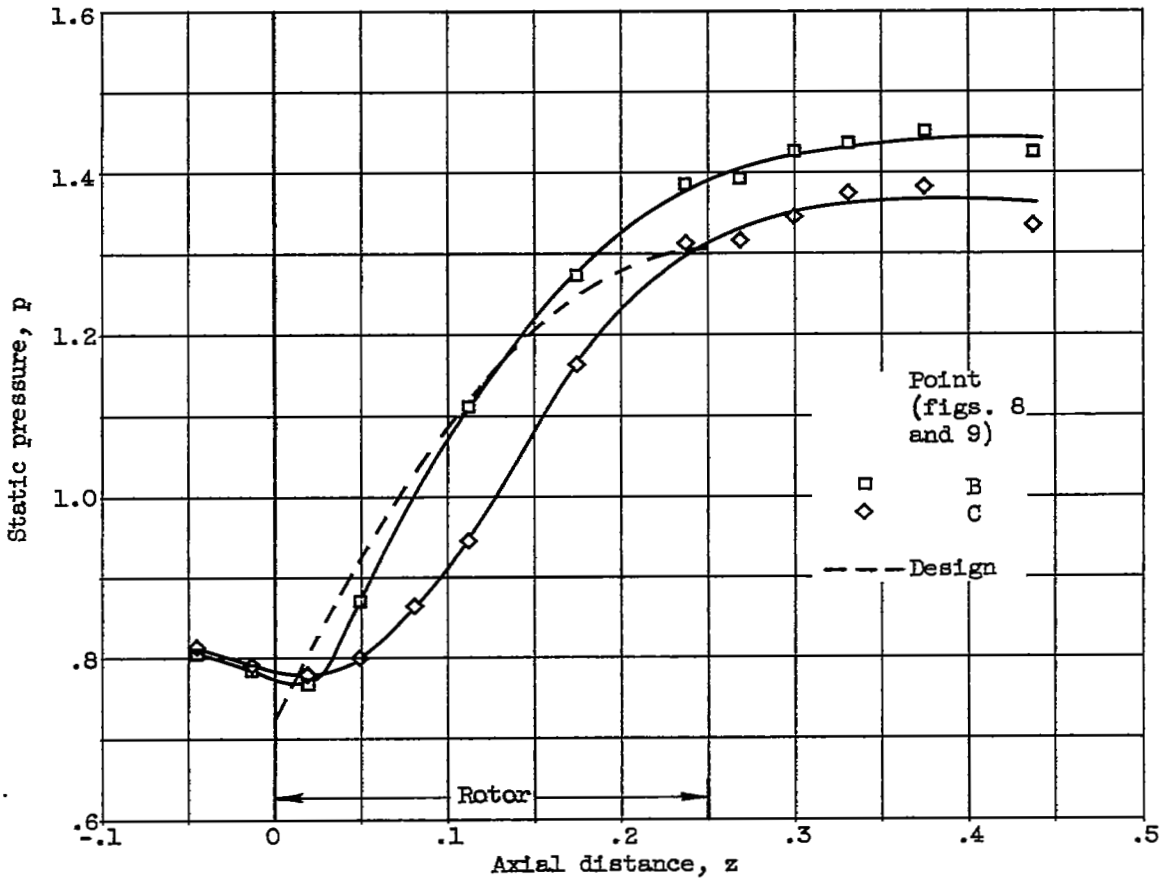

Figure 17. - Design and experimental static-pressure variation along outer wall at design speed.

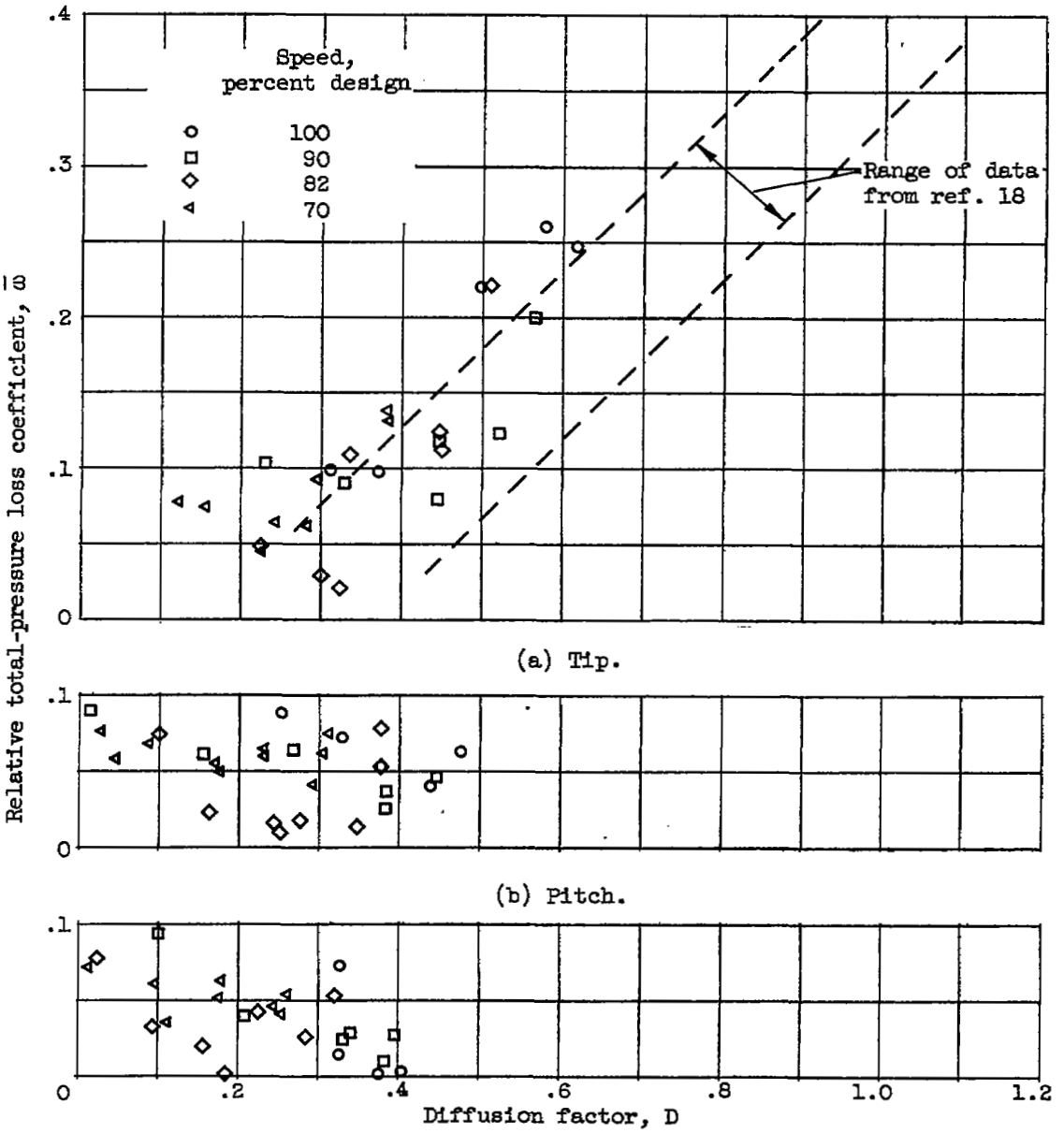

Figure 18. - Variation of rotor-blade-element losses with diffusion factor in low-loss range of incidence angle.

NACA-Langley - 4-11-55 - 325